PHYSICAL REVIEW D **79,** 124008 (2009)

Black/white hole radiation from dispersive theories

Jean Macher* and Renaud Parentani†

Laboratoire de Physique Théorique, CNRS UMR 8627, Bâtiment 210, Université Paris-Sud 11, 91405 Orsay Cedex, France

(Received 13 March 2009; published 8 June 2009)

We study the fluxes emitted by black holes when using dispersive field theories. We work with stationary one-dimensional backgrounds which are asymptotically flat on both sides of the horizon. The asymptotic fluxes are governed by a 3×3 Bogoliubov transformation. The fluxes emitted by the corresponding white holes are regular and governed by the inverse transformation. We numerically compute the spectral properties of these fluxes for both sub- and superluminal quartic dispersion. The leading deviations with respect to the dispersionless flux are computed and shown to be governed by a critical frequency above which there is no radiation. Unlike the UV scale governing dispersion, its value critically depends on the asymptotic properties of the background. We also study the flux outside the robust regime. In particular we show that its low-frequency part remains almost thermal but with a temperature which significantly differs from the standard one. Applications to four-dimensional black holes and Bose-Einstein condensates are in preparation.

DOI: 10.1103/PhysRevD.79.124008 PACS numbers: 04.70.Dy, 04.60.Bc, 43.35.+d

I. INTRODUCTION

In 1981, Unruh showed [1] that the phonon field equation in a nonhomogeneous flow is analogous to that of a relativistic field propagating in a four-dimensional curved space-time. He also suggested that this analogy could be used to experiment black hole (BH) radiation in the lab. However, as pointed out in [2], this analogy is limited by the fact that in condensed matter the phonon field becomes dispersive above a certain wave vector, say Λ. Motivated by this remark, Unruh numerically showed that the fluxes emitted by an acoustic black hole are not significantly affected by the dispersive properties of the phonons, at least when $\Lambda \gg \kappa$, where κ is the gradient of the fluid velocity at the sonic horizon [3]. Since then, this robustness of the fluxes has been confirmed both by algebraic [4–9] and numerical [10,11] techniques.

However, many open questions remain. In particular, little is known about

(i) the exact nature and the precise range of the parameters delimiting the robust regime,
(ii) the scaling properties of the leading deviations in the robust regime,
(iii) the properties of the fluxes outside this regime, and
(iv) the comparison of sub- and superluminal dispersion.

In view of the possibility to detect Hawking radiation in the lab [12], it is important to provide quantitative estimates of the modifications of the fluxes induced by dispersion. Besides this reason, answering the above questions is also relevant when exploring the consequences on black hole physics due to violations of Lorentz invariance [2,13–16] that could stem from (or be related to) quantum gravity. This could be true, in particular, when considering the signals emitted during the evaporation of light black holes ($M \sim 10^{-16}$ Planck mass) that could be produced at the LHC [17].

In this paper, we aim to answer these questions by a two step analysis. First we provide a complete description of the quantum propagation of a dispersive field in stationary black hole geometries. (To our knowledge, this has not been presented anywhere.) Secondly, focusing on quartic dispersion and using numerical methods, we study both the small modifications of the fluxes induced by dispersion when $\Lambda \gg \kappa$, and the larger modifications when this inequality is not satisfied.

We are planning to extend this work in two directions, first to Bose condensates where the phonon field obeys the Bogoliubov–de Gennes equation which differs from the ''scalar'' field equation we consider below (this program has been completed during the publication process of the present work [18]), and secondly to 4D black holes where the gravitational potential induces gray body factors which could play a critical role.

In Sec. II, we present the class of velocity profiles and the stationary mode equation. In Sec. III, we study the algebraic properties of the modes and the Bogoliubov transformation one is dealing with. In Sec. IV, we present our numerical treatment. In Secs. V and VI, we numerically solve the mode equation and interpret the results for sub- and superluminal quartic dispersion, respectively. We conclude in Sec. VII.

II. THE SETTINGS

A. Velocity profiles

We work in two space-time dimensions and consider stationary black hole geometries. These shall be charac-

*jean.macher@th.u-psud.fr
†renaud.parentani@th.u-psud.fr

terized by the velocity profile $v(x)$:

$$ds^2 = -dt^2 + (dx - v(x)dt)^2. \quad (1)$$

This expression appears [1] when considering the propagation of low-frequency phonons in a moving fluid whose velocity field $v(x)$ is measured in the Galilean frame (not necessarily the lab frame) where v only depends on x. The sound velocity is assumed to be constant and has been set to 1. A more general case will be considered in [18]. The above metric possesses an event horizon where the flow becomes supersonic.

When the fluid flows to the left, $v < 0$, and when $|v|$ increases toward the left, one obtains a future (BH) horizon. Had we considered the flow $-v(x)$, we would have obtained a white hole (WH) geometry. As we shall see, the spectral properties (in terms of the conserved frequency $\omega = i\partial_t$) of fluxes emitted by this WH are in one-to-one correspondence with those of the fluxes emitted by the BH governed by $v(x)$. However, they differ slightly. It should also be pointed out that, since we only consider dispersive mode equations, see e.g. Eq. (5), $-\infty < t, x < \infty$ in Eq. (1) represents the whole space-time [19], and not only a part of it as would have been the case when using relativistic fields.

We shall also assume that v becomes asymptotically constant on both sides of the horizon. The existence of two asymptotic regions is important because one then has well-defined asymptotic modes on *both sides*, and therefore well-defined particle fluxes. This is particularly relevant for the proposal [20,21] based on measurements of the long distance correlations [22,23] between Hawking quanta and their partners propagating on the other side of the horizon.

In order to determine the *generic* consequences of dispersion, we shall consider a large class of flows. In contrast with the nondispersive case where they play no role, we shall see that the asymptotic properties of $v(x)$ are crucial when using nonlinear dispersion relations. This will imply, in particular, that the inequality $\Lambda \gg \kappa$ is not sufficient to guarantee no significant deviation from the standard fluxes.

The class we shall use generalizes that of [10] and contains profiles of the form

$$v(x) = -1 + D\,\mathrm{sign}(x)\tanh^{1/n}\left[\left(\frac{\kappa|x|}{D}\right)^n\right]. \quad (2)$$

When changing n and D, κ, the slope of v at the horizon, is fixed, as is the location of the horizon at $x = 0$. When using the 2D massless relativistic theory, the emitted spectrum only depends on κ. Instead, when using dispersive theories, together with the ratio Λ/κ, both n and D also affect the properties of the fluxes. Figure 1 shows $v(x)$ for several values of D and n, as a function of κx.

The power n controls the sharpness of the transition from the linear behavior of v near the horizon to the asymptotic flat region. For $n \to \infty$, the transition becomes sharp. When using dispersive theories, sharp transitions give rise to nonadiabatic effects which produce superimposed oscillations [10]. Unless said otherwise, n is equal to 2 in the following.

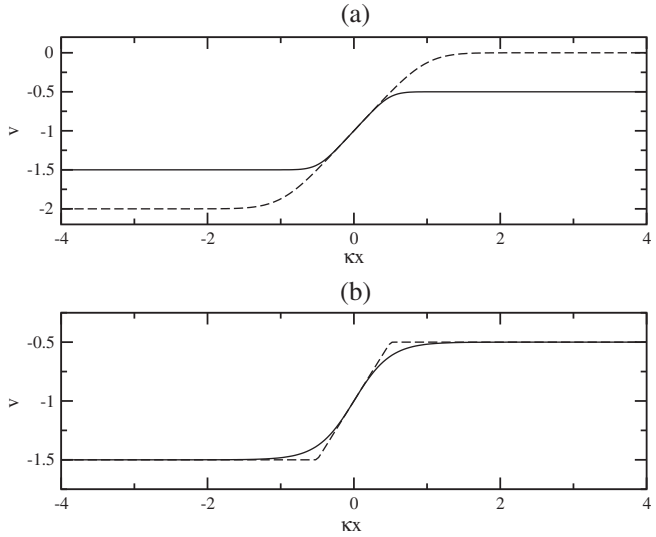

FIG. 1. Velocity profile $v(x; \kappa, n, D)$ as a function of κx. (a) n fixed to 2, $D = 0.5$ (solid line) and $D = 1$ (dashed line). (b) D fixed to 0.5, $n = 1$ (solid line), $n = 20$ (dashed line).

The parameter $D \in]0, 1]$ fixes the asymptotic values of the velocities,

$$v_\pm = -1 \pm D, \quad (3)$$

for $x \to \pm\infty$, respectively. When using nonlinear dispersion relations, D fixes the critical frequency $\omega_{\max}$ above which the radiation vanishes. This is relevant because D is constrained to be much smaller than 1 in some proposals of experiments [24]. More generally, we shall find that $\omega_{\max}$ is the most relevant parameter, in that the corrections induced by dispersion are essentially governed by $\kappa/\omega_{\max}$, and not by κ/Λ as one might have expected.

B. Dispersive wave equation

In nature of course, various dispersion relations are found depending on the condensed material used. However, when imposing analyticity in k^2, quartic dispersion relations represent the first two possible deviations from the linear case. (Dissipative theories constitute another class that should be considered separately [25,26].) In this paper, we shall thus restrict our numerical analysis to

$$\Omega^2 = k^2 \pm \frac{k^4}{\Lambda^2}, \quad (4)$$

where Ω and k are the energy and momentum measured in the frame comoving with the flow.

When working with the metric of Eq. (1) the corresponding wave equation for the velocity potential ϕ reads [3]

$$(\partial_t + \partial_x v)(\partial_t + v\partial_x)\phi = \left(\partial_x^2 \mp \frac{1}{\Lambda^2}\partial_x^4\right)\phi \qquad (5)$$

when assuming that the fluid density is constant. (This restriction will also be removed in [18].) The upper (lower) sign corresponds to super- (sub-) luminal dispersion. The conserved scalar product takes the form

$$(\phi_1, \phi_2) = i\int_{-\infty}^{\infty} dx[\phi_1^*(\partial_t + v\partial_x)\phi_2 - \phi_2(\partial_t + v\partial_x)\phi_1^*]. \qquad (6)$$

It is independent of the dispersion and it coincides with the standard Klein-Gordon (KG) product evaluated on the preferred time slices specified by dispersion (here $t = cst$).

Since the flow is stationary, we shall work at fixed (Killing) frequency ω. Setting $\phi = e^{-i\omega t}\phi_\omega(x)$ in the wave equation yields

$$(-i\omega + \partial_x v)(-i\omega + v\partial_x)\phi_\omega = \left(\partial_x^2 \mp \frac{1}{\Lambda^2}\partial_x^4\right)\phi_\omega. \qquad (7)$$

As usual, the scalar product is block diagonal in ω. Therefore, when working with stationary states, all observables will be expressed as sums of observables defined at fixed ω. More precisely, one should consider the couple of frequencies $(\omega, -\omega)$ since opposite values of ω mix in stationary Bogoliubov transformations. In what follows, to avoid any confusion, ω is always positive definite.

Before numerically studying the solutions of Eq. (7), it is worth analyzing the enlarged set of solutions and the Bogoliubov transformation one obtains.

We remind the reader that the oscillatory solutions to Eq. (7) can be classified according to the sign of their group velocity in the comoving frame, $v_{gr}^{\rm com} = d\Omega/dk$. In the following we call the modes with $v_{gr}^{\rm com} < 0$ left movers and those with the opposite sign right movers. In the absence of dispersion (and for 2D massless fields), these two sectors are decoupled, and the Bogoliubov transformation is particularly simple. When introducing (quartic) dispersion, four independent solutions to Eq. (7) exist. The classification between left and right movers can still be done, but the left-right decoupling is lost. It is worth mentioning that, when considering a varying speed of sound rather than a varying flow velocity, see e.g. [21], this decoupling is lost even in the long wavelength approximation (i.e. without dispersion). Notice also that one can introduce dispersion in a way that preserves this factorization [4,27], but these models do not seem to govern condensed matter systems.

III. ANALYTIC STUDY

In several aspects, the material presented below closely follows what has been presented in [10]. The novelties are related to the fact that we treated both asymptotic regions on an equal footing. In particular, we establish the complete character of the "in" and "out" mode bases, and we write the unitary Bogoliubov transformation which governs the general case (for stationary, one-dimensional, single horizon geometries). Finally, we show how to relate the fluxes emitted by black and white holes.

A. Asymptotic solutions

Given our velocity profile, v is asymptotically constant in both regions $|\kappa x| \gg D$. There, the solutions of Eq. (7) are superpositions of plane waves e^{ikx} with constant amplitudes. To characterize a solution, one needs the roots $k(\omega)$ of the asymptotic wave vectors and the amplitudes A_k of the corresponding waves. Owing to the nonlinearity of the dispersion relation, in addition to the oscillatory modes, exponentially growing/decaying modes governed by complex values of k exist.

We first study how to handle these extra modes in the present settings, paying attention to the completeness of the mode basis. To be specific, we concentrate on superluminal cases, and only indicate the (small) differences that arise in subluminal cases. Let us thus analyze the roots of

$$(\omega - v_\pm k)^2 = k^2 + \frac{k^{2p+2}}{\Lambda^{2p}} = \Omega^2(k) \qquad (8)$$

for $\omega > 0$, and for an arbitrary value of the integer $p > 0$. We work with a polynomial form so as to know the number of complex roots of Eq. (8). For everything concerning the real roots, nothing changes if one uses any strictly convex function $\Omega^2(k)$ with a slope equal to 1 for low k.

In the subsonic region, $|v_+| < 1$, as can be seen in Fig. 2, two real roots exist: $k_\omega^u > 0$ and $k_\omega^v < 0$, which correspond to a right and a left mover, respectively. (Whenever an ambiguity could exist, we shall add a superscript u or v to designate right or left movers.) p pairs of complex conjugated roots also exist, since the equation is real. One thus has p roots with a positive imaginary part (which corre-

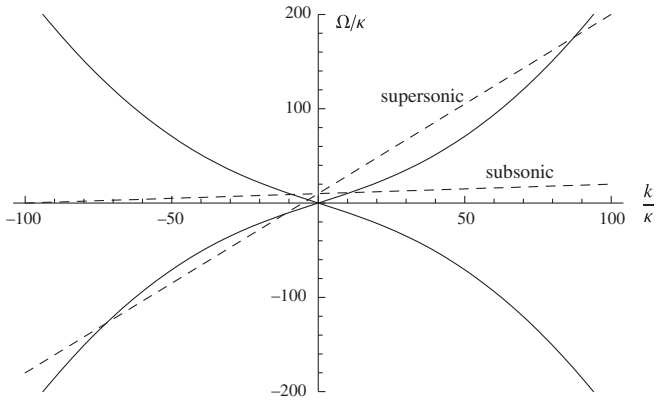

FIG. 2. The two straight lines represent $\omega - v_+ k$ for the subsonic one and $\omega - v_- k$ for the supersonic one. The roots of Eq. (8) correspond to the abscissa of the intersections of these lines with the curves $\pm\Omega(k)$. The numerical values are $p = 1$ (quartic dispersion), $\Lambda/\kappa = 50$, $D = 0.9$, and $\omega/\kappa = 10$.

spond to growing modes to the right) and p solutions with a negative imaginary part (decaying modes).

In the supersonic region $|v_-| > 1$, for ω smaller than a critical frequency $\omega_{\max}$ (we shall compute its value below), four real roots exist (see Fig. 2), and thus only $p-1$ pairs of complex solutions. In other words, when comparing this with what prevailed in the subsonic region, a pair of growing and decaying modes has been replaced by a couple of oscillatory modes. Such replacements of pairs of modes is a generic feature of quantum field theory in external fields; see the Appendix of [28]. In the present hydrodynamical settings it will occur at all horizons (for both black and white holes). For flows to the left, $v < 0$, the two new real roots both correspond to right movers. Notice that for subluminal dispersion, the replacement occurs the other way around since the four real roots are found where the flow is subsonic.

Now, given that there are $2p+2$ roots, the general solution $\phi_\omega(x)$ is a superposition of $2p+2$ modes. However, when considering the Fourier transform of the field operator, $\hat{\phi}_\omega(x)$, only a subclass of these should be used. And this subclass is *complete* in a precise sense we explain below. (To our knowledge, this crucial aspect has not been discussed in the context of acoustic black holes.) To establish the completeness of the mode basis we first need to compute the frequency $\omega_{\max}$ which is introduced by both sub- and superluminal dispersion, and which will cut off Hawking radiation.

B. Maximal frequency

The frequency $\omega_{\max}$ is the value of ω where the two extra real roots merge into each other. It is thus reached when the straight line $\omega - v_- k$ is tangent to $-\Omega(k)$, as illustrated in Fig. 3, or equally when $-|\omega| - v_- k$ is tangent to Ω, where Ω is the square root of the right-hand side of Eq. (8).

Restricting attention to quartic dispersion, the corresponding value of k is

$$k_{\max,+} = \frac{\Lambda}{2\sqrt{2}}\sqrt{v_-^2 - 4 + |v_-|\sqrt{v_-^2+8}}. \qquad (9)$$

The frequency $\omega_{\max}$ is then obtained from Eq. (8). It is thus of the form

$$\omega_{\max,+} = \Lambda f_+(D). \qquad (10)$$

For $D \ll 1$, one has $f_+(D) \propto D^{3/2}$. This means that, whatever the value of the dispersion scale Λ, $\omega_{\max,+}$ can be arbitrarily small, and, in particular, it could be even smaller than the temperature $\kappa/2\pi$ one would get in a dispersionless theory.

For subluminal dispersion, the maximal frequency $\omega_{\max,-}$ is again defined by the merging of the two extra real roots. In this case it occurs where $|v_+| < 1$. In the quartic case the corresponding value of k is

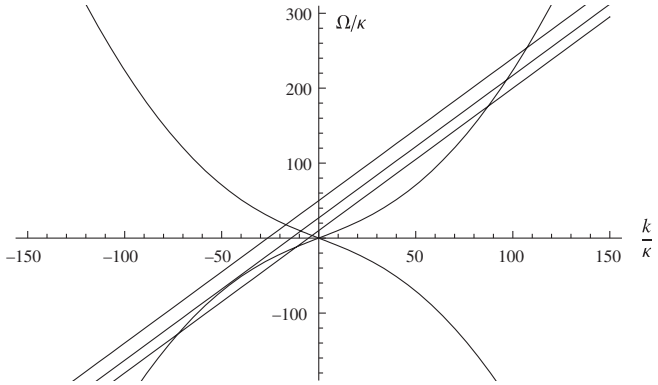

FIG. 3. Solutions to Eq. (8) in the supersonic region, for different values of ω. For $\omega < \omega_{\max}/\kappa$, two roots exist in the bottom left quadrant. They move closer to one another as ω increases and merge when the straight line $\omega - kv_-$ becomes tangent to $-\Omega(k)$, for $\omega = \omega_{\max}$. For $\omega > \omega_{\max}$, these roots no longer exist.

$$k_{\max,-} = \frac{\Lambda}{2\sqrt{2}}\sqrt{4 - v_+^2 - |v_+|\sqrt{v_+^2+8}}. \qquad (11)$$

Thus $\omega_{\max,-}$ is also of the form $\omega_{\max,-} = \Lambda f_-(D)$. For $D \ll 1$, we again obtain $f_-(D) \propto D^{3/2}$.

Figure 4 shows the contours of constant $\omega_{\max}$ in the plane (D, Λ), for sub- and superluminal dispersion. The

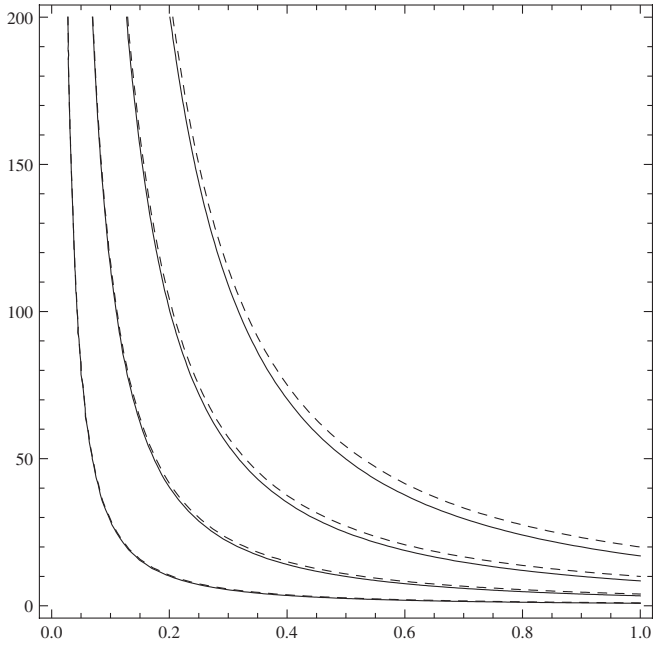

FIG. 4. Contours of constant $\omega_{\max}$ in the plane $(D, \Lambda/\kappa)$. D is the horizontal coordinate, Λ/κ the vertical one. From left to right, the contours correspond to $\omega_{\max}/\kappa = 0.5$, 2, 5, and 10. The solid contours are for superluminal dispersion and the dashed ones for subluminal dispersion. The contours coincide for small D, and so do the functions f_+ and f_-. Their difference becomes visible as D grows.

same value of $\omega_{\max}/\kappa$ can be obtained with very different combinations of $(D, \Lambda/\kappa)$. As we shall see in Sec. V, the fluxes are highly degenerate on these contours, which means that the corrections with respect to the standard fluxes are essentially governed by $\omega_{\max}/\kappa$.

C. Mode orthonormality and mode completeness

To proceed to the canonical quantization, one should use mode bases that are orthonormal and complete. When the background geometry is homogeneous, this is rather easy, even in the presence of dispersion. However, when v of Eq. (1) varies and, in particular, when it characterizes a horizon, it becomes trickier. Let us thus first consider situations where v is constant both in space and time.

1. Homogeneous metrics, k representation

In this case one should exploit the homogeneity and express the field operator in terms of exponentials e^{ikx} and creation/destruction operators labeled by (real) k

$$\hat{\phi}(t,x) = \int_{-\infty}^{\infty} \frac{dk}{\sqrt{2\pi}} \left[\hat{a}_k e^{ikx} \frac{e^{-i\omega t}}{\sqrt{2\Omega(k)}} + \text{H.c.} \right], \tag{12}$$

where $\omega = \Omega(k) + vk$ with $\Omega(k)$ given in Eq. (8). In this representation, creation/destruction operators obey the usual commutators $[\hat{a}_k, \hat{a}^\dagger_{k'}] = \delta(k-k')$. In addition, the modes which multiply these operators in Eq. (12) are orthonormal: their norm, Eq. (6), is $\delta(k-k')$, *irrespective* of both whether v is sub- or supersonic, and the choice of the dispersion relation (8)[1].

The completeness of the mode basis is needed to verify that the equal time commutator

$$[\hat{\phi}(t,x), \hat{\pi}(t,x')] = i\delta(x-x') \tag{13}$$

is satisfied when $\hat{\phi}$ is given in Eq. (12) and where $\hat{\pi} = (\partial_t - v\partial_x)\hat{\phi}$. In the present representation, the proof is easily obtained by making use of the completeness (in the sense of Fourier analysis) of the exponentials e^{ikx}, with k real from $[-\infty, \infty]$. It should be stressed that the proof applies to all dispersion relations and to all (constant) values of v, both sub- and supersonic.

When considering nonhomogeneous stationary flows one must use the conserved frequency ω in place of the wave vector k to label modes and operators. So, in preparation for this case, let us study the change of representation from k to ω in homogeneous flows.

[1]In the case of subluminal dispersion, there could exist a maximal value of k associated with the vanishing of $\Omega^2(k)$. In this case, the mode basis is no longer complete in a Fourier sense. To deal with this, one can either work [29] with "regularized" dispersion relations which do not develop imaginary values of Ω, or with a "Bloch waves" perspective [30] where Ω is periodic in k space.

2. Homogeneous metrics, the ω representation

The above conclusion concerning the completeness character of the modes implies that, in any homogeneous flow, the "extra" (growing and decaying) solutions of the mode equation at fixed ω must be discarded when quantizing $\hat{\phi}$. When the flow is subsonic, using the dispersion relation (8), one should thus discard the $2p$ growing/decaying modes, whereas when the flow is supersonic, one should discard only $2(p-1)$ modes. Because of this, the change of representation from k to ω should be done separately in sub- and supersonic regions.

Let us first consider the subsonic case where only two real roots exist. For each $\omega > 0$, one has two modes:

$$\varphi^i_\omega(x) = \sqrt{\frac{dk^i}{d\omega}} \frac{e^{ik^i x}}{\sqrt{4\pi\Omega(k^i)}}, \tag{14}$$

where $k^i = k^i(\omega)$, $i = u, v$, are the two real roots of Eq. (8) describing the right- and left-moving modes. These modes obey Eq. (7) and are orthonormal for the KG product, in the sense of a Dirac distribution $\delta(\omega - \omega')$. Correspondingly, one has the rescaled annihilation operators:

$$\hat{a}^{\,i}_{\omega} = \sqrt{\frac{dk^i}{d\omega}} \hat{a}_{k^i}, \tag{15}$$

which verify $[\hat{a}^i_\omega, \hat{a}^{j\dagger}_{\omega'}] = \delta^{ij}\delta(\omega-\omega')$. Using these modes, the integral in Eq. (12) can be rewritten as

$$\hat{\phi}(t,x) = \int_0^\infty d\omega [e^{-i\omega t}\hat{\phi}_\omega + \text{H.c.}], \tag{16}$$

$$\hat{\phi}_\omega = \varphi^u_\omega(x)\hat{a}^u_\omega + \varphi^v_\omega(x)\hat{a}^v_\omega. \tag{17}$$

The family of modes (14) is complete, because the exponentials e^{ikx} are.

When the flow is supersonic, the situation is trickier because the Jacobian $dk/d\omega$ crosses zero for right movers. Nevertheless, similar results are obtained. Namely, as above, one first separates the integral $\int_{-\infty}^{\infty} dk$ in Eq. (12) into two integrals over a u and a v sector. When considering the v sector ($k < 0$) in left-moving flows $v < 0$, nothing changes because $dk/d\omega$ does not cross zero. Therefore, all left-moving (positive norm) modes can still be uniquely described by ω belonging to $[0, \infty]$, and the change of variable $k \to \omega$ can be made without further precaution.

The same is no longer true for the right-moving sector. In fact, the integral over the right movers $\int_0^\infty dk$ splits into an integral over ω belonging to $[0, \infty]$ plus another piece over negative frequencies belonging to $[-\omega_{\max}, 0]$. In addition, for a given value of $\omega < 0$ in this interval, two real roots $k^u(\omega) > 0$ exist. It ends when the two roots merge into each other when $-\omega_{\max}$ is reached.

Thus, for $\omega > \omega_{\max}$, one has only one (positive norm) u root and $\hat{\phi}_\omega$ reads as in Eq. (17). Instead, when $0 < \omega < \omega_{\max}$, three real roots exist: the continuation (in ω) of the

former positive norm one, and two new roots with negative Ω, and thus negative norm; see Fig. 3. In this case, $\hat{\phi}_\omega$ must be decomposed as

$$\hat{\phi}_\omega = \hat{a}^u_\omega \varphi^u_\omega + \hat{a}^v_\omega \varphi^v_\omega + \sum_{l=1,2} \hat{a}^{u\dagger}_{-\omega,l} (\varphi^u_{-\omega,l})^*. \quad (18)$$

When compared with Eq. (17), the last two terms describe the two new roots. A complex conjugate and a subscript $-\omega$ have been used to characterize the modes which multiply the creation operators $\hat{a}^\dagger_{-\omega,l}$. This means that the modes $\varphi^u_{-\omega,l}$ have a positive norm and obey the mode equation with a frequency $i\partial_t = -\omega < 0$.

Using the Fourier operator $\hat{\phi}_\omega(x)$ of Eq. (18), containing both annihilation and creation sectors, the field $\hat{\phi}(t, x)$ can still be written as in Eq. (16), as an integral over $\omega \in [0, \infty]$.

3. Inhomogeneous metrics

In metrics which contain a transition from a subsonic to a supersonic flow, the decomposition of $\hat{\phi}_\omega$ is modified: because of the scattering on $v(x)$, the asymptotic modes used above mix into each other and with the growing and decaying modes. As explained in the Appendix, when excluding the growing modes, there is a change in the dimensionality of the mode bases. Indeed, instead of Eq. (18), for $0 < \omega < \omega_{\max}$, $\hat{\phi}_\omega$ now reads

$$\hat{\phi}_\omega(x) = \hat{a}^u_\omega \varphi^u_\omega(x) + \hat{a}^v_\omega \varphi^v_\omega(x) + \hat{a}^{u\dagger}_{-\omega}(\varphi^u_{-\omega}(x))^*. \quad (19)$$

We have introduced only one extra mode, and not two, because the combination of the former two $\varphi^u_{-\omega,l}$ that is orthogonal to the above $\varphi^u_{-\omega}$ in the asymptotic supersonic region is unbounded in the subsonic region. This is very similar to what is found with the Airy function: only one combination of two oscillatory modes in the allowed region remains bounded in the forbidden region.

For $\omega > \omega_{\max}$ instead, nothing changes and $\hat{\phi}_\omega$ should still be decomposed as in Eq. (17) because one has two (positive norm) real roots for all x.

When considering subluminal dispersion, the situation is similar but with several changes. For $0 < \omega < \omega_{\max}$, there are four real roots in the asymptotic *subsonic* part of the flow, and the mode operator $\hat{\phi}_\omega$ should be decomposed again as in Eq. (19). The difference with superluminal dispersion is that the two additional roots are associated with the first term $\hat{a}^u_\omega \varphi^u_\omega$ and no longer with the third one.

D. Bogoliubov transformation

For stationary flows and stationary states, the properties of the fluxes are all encoded in a (ω-block-diagonal) Bogoliubov transformation. This relates the in modes $\varphi^{\text{in}}_\omega$, $\varphi^{\text{in}}_{-\omega}$, which are associated with the destruction operators annihilating the initial vacuum state, to the out modes $\varphi^{\text{out}}_\omega$, $\varphi^{\text{out}}_{-\omega}$ which characterize the asymptotic particle content of the fluxes.

To obtain the asymptotic temporal behavior of the modes from their asymptotic spatial behavior, it suffices (see e.g. Sec. 1.3 in [23]) to consider wave packets centered about the value of ω under examination. In what follows we shall not distinguish single frequency modes from the corresponding broad wave packet. Therefore, when discussing the initial (or final) behavior of a mode, it should be understood as that of the corresponding wave packet.

Given that the flow v becomes asymptotically constant for large $|x|$, the identification of in and out modes is free of ambiguity. The in (respectively, out) modes are defined as the modes with positive comoving frequency Ω in the asymptotic past (respectively, future) and in the regions where the flow is homogeneous. They are separated into u, in modes (respectively, u, out modes) with $d\Omega/dk > 0$ in the asymptotic past (respectively, future), and v, in (respectively, v, out) modes with $d\Omega/dk < 0$. These conditions fix uniquely the complete set of 3 in (respectively, out) modes. In this work, the state of the field is taken to be the in vacuum, annihilated by the a^{in}_ω associated with the in modes. Physically, it corresponds to a state devoid of particles propagating toward the horizon in the regions where v is constant. Notice finally that this definition of the in vacuum does not coincide with that of the ''Unruh vacuum'' [31] which rests on the use of relativistic fields, and of an affine null parameter on the past horizon.

1. Simplified case

To see what the new aspects brought in by dispersive effects are, let us briefly describe the Bogoliubov transformation when assuming that the left-moving piece $\hat{a}^v_\omega \phi^v_\omega$ in Eqs. (17) and (19) decouples from the right-moving sector. In this case it is sufficient to consider only one relation among u modes, for instance that with $\omega > 0$

$$\varphi^{u,\text{in}}_\omega = \alpha_\omega \varphi^{u,\text{out}}_\omega + \beta_\omega (\varphi^{u,\text{out}}_{-\omega})^*. \quad (20)$$

Indeed, the norm of β_ω is given by both overlaps

$$|\beta_\omega|^2 = |(\varphi^{u,\text{out}*}_{-\omega}, \varphi^{u,\text{in}}_\omega)|^2 = |(\varphi^{u,\text{out}*}_\omega, \varphi^{u,\text{in}}_{-\omega})|^2. \quad (21)$$

This square fixes the mean occupation number of phonons (found in the in vacuum) for both positive and negative frequencies: $\bar{n}_\omega = \bar{n}_{-\omega} = |\beta_\omega|^2$. In fact, since each produced pair contains one quantum of frequency ω and its partner of frequency $-\omega$, there is no need to differentiate between these two occupation numbers. We emphasize this simple property because it will be lost when the coupling to v modes is no longer neglected.

A significant difference due to dispersion is that $\bar{n}_\omega = 0$ for $\omega > \omega_{\max}$ because there is no bounded mode $\varphi^u_{-\omega}$ for superluminal dispersion (no φ^u_ω for subluminal dispersion).

2. General case with $u - v$ mixing

Taking into account the coupling between right- and left-moving modes, the above situation changes as follows.

For $\omega > \omega_{\max}$, one still has $\bar{n}_\omega = 0$. However, the remaining two modes are scattered by the potential, and this is described by a single equation

$$\varphi_\omega^{u,\text{in}} = T_\omega \varphi_\omega^{u,\text{out}} + R_\omega \varphi_\omega^{v,\text{out}}, \tag{22}$$

where $|T_\omega|^2 + |R_\omega|^2 = 1$. One thus has an elastic scattering of u and v modes, without spontaneous pair creation.

For $\omega < \omega_{\max}$, unlike what was found in Eq. (20), three equations are now needed to characterize the Bogoliubov transformation between in and out modes

$$\begin{aligned}
\varphi_\omega^{u,\text{in}} &= \alpha_\omega \varphi_\omega^{u,\text{out}} + \beta_{-\omega}(\varphi_{-\omega}^{u,\text{out}})^* + \tilde{A}_\omega \varphi_\omega^{v,\text{out}},\\
\varphi_\omega^{v,\text{in}} &= \alpha_\omega^v \varphi_\omega^{v,\text{out}} + B_\omega(\varphi_{-\omega}^{u,\text{out}})^* + A_\omega \varphi_\omega^{u,\text{out}},\\
\varphi_{-\omega}^{u,\text{in}} &= \alpha_{-\omega} \varphi_{-\omega}^{u,\text{out}} + \beta_\omega(\varphi_\omega^{u,\text{out}})^* + \tilde{B}_\omega(\varphi_\omega^{v,\text{out}})^*.
\end{aligned} \tag{23}$$

As usual, the coefficients are given by the KG overlap of the corresponding (normalized) in and out modes, e.g. $\beta_\omega = -(\varphi_\omega^{u,\text{out}*}, \varphi_{-\omega}^{u,\text{in}})$. Using the mode orthonormality, their normalization immediately follows, e.g. for the first equation one gets $|\alpha_\omega|^2 - |\beta_{-\omega}|^2 + |A_\omega|^2 = 1$. In these expressions, the minus signs come from complex conjugated, negative norm, modes.

When working in the in vacuum, the occupation numbers of out quanta, are, respectively,

$$\begin{aligned}
\bar{n}_\omega &= |\beta_\omega|^2, \qquad \bar{n}_\omega^v = |\tilde{B}_\omega|^2,\\
\bar{n}_{-\omega} &= |\beta_{-\omega}|^2 + |B_\omega|^2 = \bar{n}_\omega + \bar{n}_\omega^v.
\end{aligned} \tag{24}$$

To obtain these expressions one needs to compute the in-in expectation value of the corresponding out occupation number operator. The three expressions follow when decomposing the out operators in terms of in ones, and using relations among Bogoliubov coefficients.

Several remarks should be made. First, to get these expressions we have treated the quanta emitted to the right, which correspond to the outgoing Hawking radiation and which are described by $\varphi_\omega^{u,\text{out}}$, on the same footing as those emitted to the left which are described by $\varphi_\omega^{v,\text{out}}$ and $\varphi_{-\omega}^{u,\text{out}}$. When v is asymptotically constant on both sides, there is no reason to treat them differently.

Secondly, because of the $u - v$ coupling, the numbers of u quanta in general differ: $\bar{n}_{-\omega} \neq \bar{n}_\omega$. In fact the meaning of $\bar{n}_{-\omega} = \bar{n}_\omega + \bar{n}_\omega^v$ is clear. It tells us that two channels exist to spontaneously produce u quanta of frequency $-\omega$: either through the usual channel where the partner is a Hawking quantum reaching $x = \infty$, or through the new channel where the partner is a v mode. When this B channel is negligible, i.e. when $|B_\omega|^2 \ll |\beta_\omega|^2$, one recovers the former situation where $\bar{n}_{-\omega} = \bar{n}_\omega$.

The B channel was first described in [10], where it was also claimed that "this particle creation has absolutely nothing to do with black holes." We do not agree because, in our settings, there is no reason either to treat differently the production of $u - v$ pairs weighted by B_ω from Hawking radiation, i.e. the production of $u - u$ pairs weighted by β_ω. Indeed, both $\bar{n}_\omega$ and $\bar{n}_\omega^v$ are generically nonzero when (and only when) the negative frequency u modes $\varphi_{-\omega}^u$ exist[2]. More precisely, unless one deals with a 2D massless relativistic field, the coefficients B_ω do not vanish. In fact, one generically has $B_\omega \neq 0$ even when using the dispersionless mode equation of phonons in a Eulerian fluid [9,18,21].

Thirdly, there is a linear scattering between u and v modes of positive ω which is characterized by the coefficients $\tilde{A}_\omega$ and A_ω for $\omega < \omega_{\max}$ and by R_ω, T_ω for $\omega > \omega_{\max}$. This is reminiscent of the "gray body factors" which are found when considering four-dimensional black holes. However, the latter are computed on one side only of the horizon, whereas here the coefficients relate asymptotic modes defined on both sides.

Finally, we emphasize the fact that Eq. (23) describes the scattering whenever a stationary background contains a single horizon surrounded by two asymptotic homogeneous regions. It applies indeed to *all* dispersive mode equations, both for sub- and superluminal relations. It is only when the $u - v$ mixing identically vanishes that Eq. (23) reduces to Eq. (20).

E. Wave-packet propagation

It is useful to represent the above in modes. The description of out modes follows without difficulty. Let us start with $\varphi_{-\omega}^{u,\text{in}}$ in the superluminal case. This mode has the following space-time structure; see Fig. 5. Initially, one only has the incoming branch which possesses a unit norm, and whose initial wave vector is k_+^u, the largest additional real root when the flow is supersonic. At late time, one has three branches: the "reflected" negative frequency mode described by $\varphi_{-\omega}^{u,\text{out}}$ whose amplitude is $\alpha_{-\omega}$ and whose wave vector is k_-^u, the smallest new root; the produced v mode described by $(\varphi_\omega^{v,\text{out}})^*$, and the produced u mode described by $(\varphi_\omega^{u,\text{out}})^*$. We leave the description of the other in modes and of the out modes up to the reader.

From the above we can already conclude that the emission of radiation stops for $\omega > \omega_{\max}$. Indeed, in the absence of negative frequency partners, both $\bar{n}_\omega$ and $\bar{n}_\omega^v$ identically vanish above $\omega_{\max}$. The same is not true for the subluminal case. It is thus worth describing the in mode $\varphi_{-\omega}^{u,\text{in}}$ in this case; see Fig. 6. Initially, one still has only the

[2]It is appropriate to raise the question whether the existence of the negative frequency modes $\varphi_{-\omega}^u$ implies that the background is similar to that of a "black hole." In this respect it should first be pointed out that the definition of a black hole is inherently ambiguous in the presence of dispersion. Nevertheless, what is always true [in a metric as in Eq. (1)] is that whenever $\varphi_{-\omega}^u$ exists, its group velocity $d\Omega/dk$ is smaller than v in some region of space, as is the case in the inside region of a black hole when using relativistic fields.

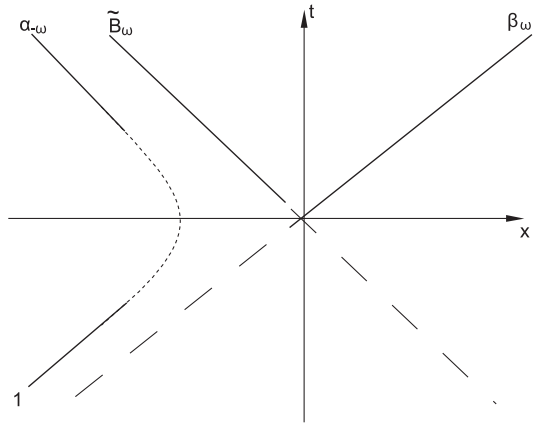

FIG. 5. Schematic space-time behavior of a wave packet made out of $\varphi^{u,\mathrm{in}}_{-\omega}$ modes, for superluminal dispersion.

incoming branch which possesses a unit norm and which has the largest positive wave vector k^u_+. At late time, one has again three branches: the transmitted negative frequency mode described by $\varphi^{u,\mathrm{out}}_{-\omega}$ whose amplitude is $\alpha_{-\omega}$, the produced v mode described by $(\varphi^{v,\mathrm{out}}_{\omega})^*$, and the produced u mode described by $(\varphi^{u,\mathrm{out}}_{\omega})^*$. When $\omega > \omega_{\mathrm{max}}$, the production of positive frequency u modes vanishes ($\bar{n}_\omega = 0$) but the "new" channel is still open. Thus, in the case of subluminal dispersion, one exactly has $\bar{n}_{-\omega} = \bar{n}^v_\omega$ for $\omega > \omega_{\mathrm{max}}$, and no longer $\bar{n}_\omega = \bar{n}_{-\omega} = \bar{n}^v_\omega = 0$ as for superluminal dispersion.

From a conceptual point of view, this completes the analysis of the black hole case. What remains to be done is to compute the coefficients of Eqs. (23). If one is only interested in the flux in the in vacuum, the knowledge of the norm of β_ω and $\tilde{B}_\omega$ is sufficient as they fix the three occupation numbers of Eq. (24).

Before performing their calculation, it is interesting to consider flows that engender white holes. Given that $-v(x)$ describes a WH geometry when $v(x)$ described a BH

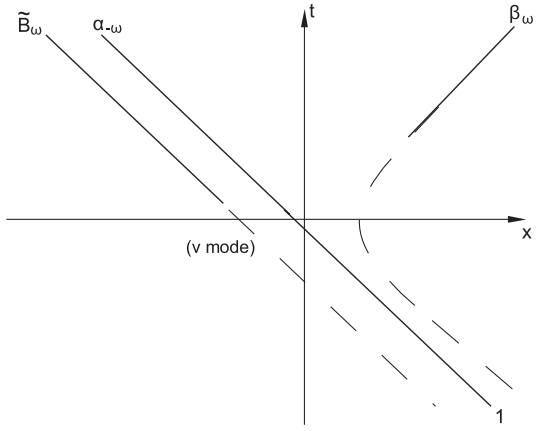

FIG. 6. Space-time behavior of $\varphi^{u,\mathrm{in}}_{-\omega}$, for subluminal dispersion.

geometry, the fluxes emitted by a WH can be algebraically related to those of the corresponding BH.

F. White holes

We first notice that the mode equation (5) is left unchanged under the double replacement $v \to -v$ and $t \to -t$. Then, in Fourier transform, the left-moving positive norm modes with fixed ω in the WH geometry are the complex conjugate of the right movers found in the corresponding BH geometry. This means that each mode has a group velocity $v_g = d\omega/dk$ opposite that of the corresponding BH mode, so that the BH in modes become out modes and vice versa.

When working in the in vacuum (defined in the same way as in the former sections), and when neglecting the coupling to the v modes, this implies no change in the occupation numbers:

$$\bar{n}^{\mathrm{WH}}_\omega = \bar{n}^{\mathrm{WH}}_{-\omega} = \bar{n}_\omega, \tag{25}$$

where $\bar{n}_\omega$ is given by $|\beta_\omega|^2$ obeying Eq. (21).

Before discussing the physical consequences of this result, let us see how it gets modified when taking into account the $u - v$ mixing. In this case the occupation numbers differ. To obtain them, it suffices to write the inverse Bogoliubov transformation of Eq. (23), and relate the coefficients of the inverse transformation to those of Eq. (23). One finds that the occupation numbers in the WH geometry governed by $-v(x)$ are *exactly* given by

$$\bar{n}^{\mathrm{WH}}_\omega = |\beta_{-\omega}|^2, \qquad \bar{n}^{u\mathrm{WH}}_\omega = |B_\omega|^2, \qquad \bar{n}^{\mathrm{WH}}_{-\omega} = \bar{n}_{-\omega}, \tag{26}$$

where the Bogoliubov coefficients are computed in the BH geometry described by $v(x)$ and where the superscript u indicates that $|B_\omega|^2$ corresponds to the occupation number of the right movers in the WH geometry.

The equality $\bar{n}^{\mathrm{WH}}_{-\omega} = \bar{n}_{-\omega}$ expresses that the (total) pair creation rate is unchanged, as must be the case because it governs the norm of the overlap between the in and out vacua. The inequality $\bar{n}^{\mathrm{WH}}_\omega \neq \bar{n}_\omega$ means that their internal repartition does not coincide. However, when $|\tilde{B}_\omega|^2 \ll |\beta_\omega|^2$, one has $\bar{n}^{\mathrm{WH}}_\omega \simeq \bar{n}^{\mathrm{WH}}_{-\omega} = \bar{n}_{-\omega}$. In this case, the WH fluxes are essentially the same as those of the corresponding BH fluxes.

Besides this close agreement, the important consequence of Eq. (26) is that dispersive theories predict that WH emit fluxes with well-defined asymptotic properties [when starting with the asymptotic in vacuum, which is well defined when $v(x)$ is asymptotically constant]. When using relativistic theories instead, one obtains an endless focusing of null geodesics toward the (past) horizon which prevents one from getting any outgoing radiation. (It should be nevertheless noticed that in the equilibrium state, in the so-called Hartle-Hawking vacuum, the stress tensor of a relativistic field is regular and the spectrum of the

particles "emitted" by the past horizon is thermal with the usual temperature, in virtue of the stationarity.)

In spite of the near equality of occupation numbers in Eq. (26), there is a major physical difference between the WH and the BH cases, which furthermore explains why dispersionless and dispersive theories behave so differently. In the WH geometry, the final values of the comoving ("proper") frequencies Ω are of the order of the UV scale Λ, whereas, in the BH case, they are of the order of $\omega \sim T_H$. This directly follows from the fact that the values of Ω and k of WH quanta are those of the ancestors of Hawking quanta. Because of this when taking the limit $\Lambda \to \infty$, i.e. the dispersionless limit, the BH fluxes are asymptotically unchanged whereas the WH ones become singular (and ill defined). This shows once more [32] that the relativistic (dispersionless) case constitutes an isolated and unstable case, as far as UV properties are concerned.

In brief, we have shown that the ill definedness of WH fluxes in relativistic theories, which is due to the unbounded character of the blue shifting effect, is properly regularized by the use of dispersion. (In this we disagree with the conclusion reached in [33].)

G. CJ modes

We now address the question of the numerical analysis of the solutions of Eq. (7). To this end, one needs to introduce yet another type of mode. We shall call them the "CJ" modes, since their usefulness for numerical analysis was first recognized in [10]. The basic reason to introduce these modes has to do with the control of the growing modes. Whereas conceptually we have demonstrated that the growing modes should be discarded from the field operator, when performing a numerical integration of Eq. (7), they will be systematically generated and will thus completely mask the physical modes. To avoid this nuisance, one should use the CJ modes. Even though they are defined essentially in the same way for sub- and superluminal dispersion, we analyze them separately because the information they carry differs.

1. Subluminal dispersion

Consider the integration from left to right of Eq. (7) starting deep in the supersonic region, i.e. on the left of the horizon, where the complex-k modes live. When reaching the horizon region, the solution is completely dominated by the mode that grows when going toward the horizon (in our terminology, we called it the decaying mode, see the Appendix). Therefore, one is effectively left with a well-defined mode, up to an overall normalization. The CJ mode is the mode which has a unit positive KG norm, and such that only the coefficient of the decaying mode is nonzero in the asymptotic region $x \to -\infty$. For $x \to \infty$ it contains four oscillatory asymptotic modes; see Fig. 7. It should be noticed that this is only true for quartic dispersion. Indeed for higher order dispersion, Eq. (8), there will still be $p-1$ growing modes which complicate obtaining a stable numerical analysis.

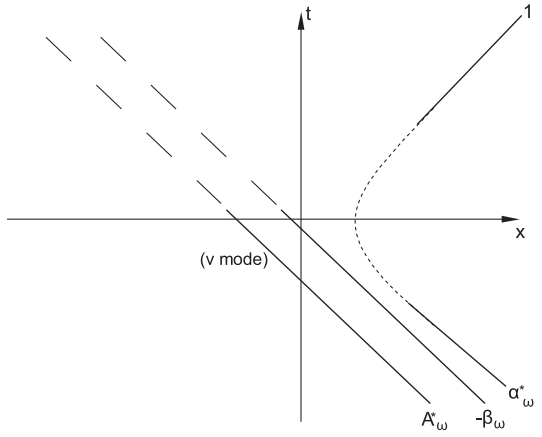

FIG. 7. Space-time behavior of $\varphi^C_\omega = \varphi^{u,\mathrm{out}}_\omega$, for subluminal dispersion.

By direct inspection, one verifies that the CJ mode corresponds to the out mode $\varphi^{u,\mathrm{out}}_\omega$. Using the conventions of Eqs. (23), one has indeed

$$\varphi^C_\omega = \varphi^{u,\mathrm{out}}_\omega = \alpha^*_\omega \varphi^{u,\mathrm{in}}_\omega - \beta_\omega (\varphi^{u,\mathrm{in}}_{-\omega})^* + A^*_\omega \varphi^{v,\mathrm{in}}_\omega. \quad (27)$$

Thus one can read off the occupation number of Hawking quanta $\bar{n}_\omega = |\beta_\omega|^2$. However, using the CJ mode, one has no access to the number of v quanta $\bar{n}^v_\omega = |\tilde{B}_\omega|^2$. To have access to $\bar{n}^v_\omega$ we shall use other modes, when the growth toward the horizon is not too strong.[3]

2. Superluminal dispersion

In the superluminal case, the situation is symmetrical with respect to the horizon, but also more complicated. The difficulty arises from the fact that the CJ mode does not correspond to an in nor an out mode, since it possesses two incoming and two outgoing waves as shown in Fig. 8. Nevertheless it is still defined as the unit positive norm solution that is purely decaying (growing toward the horizon) in the region where complex-k modes live. To have a positive norm, it must have a negative frequency. Hence we shall denote it $\varphi^C_{-\omega}$. It possesses four branches for $x \to -\infty$ with well-defined asymptotic properties: a wave packet made out of CJ modes has, at early times, the following behavior:

$$\varphi^C_{-\omega} = \alpha^C_{-\omega} \varphi^{\mathrm{in}}_{-\omega} + \beta^C_\omega (\varphi^{u,\mathrm{in}}_\omega)^*. \quad (28)$$

At late times, it behaves instead as

[3]For high values of $\omega_{\max}/\kappa$ the growth of the CJ mode is so strong that we were not able to extract information about the other modes. Instead, for $\omega_{\max}/\kappa \lesssim 2$, the growth is sufficiently mild that we could compute accurately the two oscillatory solutions and thus extract the complete Bogoliubov transformation.

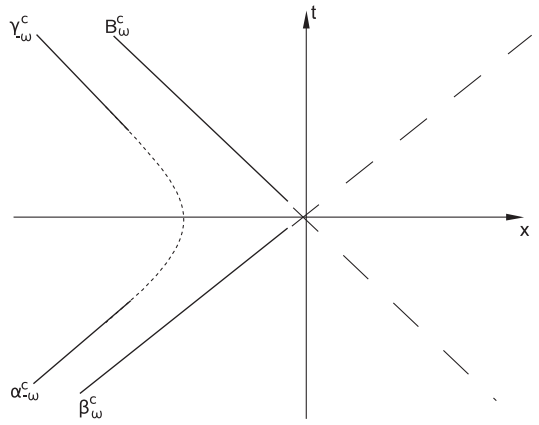

FIG. 8. Space-time behavior of $\varphi^C_{-\omega}$, for superluminal dispersion.

$$\varphi^C_{-\omega} = \gamma^C_{-\omega}\varphi^{\text{out}}_{-\omega} + B^C_\omega(\varphi^{v,\text{out}}_\omega)^*. \tag{29}$$

The coefficients obey $|\alpha^C_{-\omega}|^2 - |\beta^C_\omega|^2 = |\gamma^C_{-\omega}|^2 - |B^C_\omega|^2 = 1$.

We now have to establish the link between these coefficients and the occupation numbers of out quanta in the in vacuum. Using the above equations, one can deduce

$$\bar{n}_\omega = |\beta_\omega|^2 = |\beta^C_\omega|^2 \times (1 - |A_\omega|^2), \tag{30}$$

and

$$|B_\omega|^2 = |B^C_\omega|^2 \times \frac{|\alpha^v_\omega|^2}{1 + |B^C_\omega|^2}. \tag{31}$$

In the sequel we shall make the approximation (already used in [5]) $\bar{n}_\omega = |\beta^C_\omega|^2$ to compute the modifications induced by superluminal dispersion. This approximation shall be validated by showing that $|A_\omega|^2 \ll 1$ is verified in the whole region of the parameter space where we could compute it, and that $|A_\omega|^2$ is decreasing toward the inaccessible region.

IV. NUMERICAL PROCEDURE

A. Initial conditions

As explained above, the presence of complex roots imposes the direction of integration and the way the initial conditions are fixed. Indeed, when integrating Eq. (7) numerically, the mode growing in the direction of integration will dominate at some point the oscillatory modes. In the subluminal case, to get the CJ mode one must integrate from left to right starting from deep inside the supersonic region. For the same reason, to get the CJ mode in the superluminal case, the integration must be performed from right to left.

In addition, the imaginary part of k^C_ω characterizing the CJ mode is generically large (in units of κ) even for moderate values of D and $\lambda = \Lambda/\kappa$. For instance, for $D = 0.5$, $\lambda = 50$, and $\omega = \kappa$, and for subluminal dispersion, $|\text{Im}k^C|/\kappa \simeq 55$. This constrains how far from the horizon the initial conditions can actually be set.

In practice, the initial conditions are thus fixed as follows. At a point x_i deep into the supersonic (subsonic for superluminal dispersion) region, so that $v(x_i)$ is equal to its asymptotic value up to the machine precision (10^{-16} with the C double precision type), the value of the mode, its first, second, and third derivatives are imposed using the fact that in this asymptotic region it is equal to

$$\varphi^C_\omega = u_0 e^{ik^C_\omega(x-x_i)}. \tag{32}$$

u_0 is taken very small so that the initial exponential growth of the mode does not cause an overflow (the C double precision type is limited to the range 10^{-308}–10^{308}). Since u_0 cannot be smaller than 10^{-308}, $|x_i|$ is limited by the imaginary part of k^C. This limitation causes no problem since, as we saw, the bigger the growth of the CJ mode, the less important the precision of the initial conditions, the growth itself ensuring that any trace of unwanted excitation of the other modes quickly becomes smaller than the numerical noise.

In brief we have two regimes, either $|\text{Im}k^C|/\kappa \gg 1$ in which case the growth is strong and we have only access to the CJ mode, or $|\text{Im}k^C|/\kappa \lesssim 1$ and the growth is weak and we can compute all mode.3 Luckily, in the first case, the leading deviations with respect to the standard flux can be deduced from the CJ mode.

B. Extraction of the asymptotic coefficients

The integration is carried out from x_i to some x_f on the other side of the horizon, by an embedded 8th order Runge-Kutta-Prince-Dormand algorithm, with a relative precision of 10^{-14}. The real and imaginary parts of the numerical solution to Eq. (7) thus obtained are stored between some x_w and x_f. x_w is chosen so that it sits in the region where $v(x)$ has reached its asymptotic value. It is typically taken equal to $-x_i$. x_f is then chosen so that $|x_f - x_w|$ is equal to the period of the component with the smallest $|k|$, which on Fig. 2 is seen to be k^v, the wave vector of the v mode. There is thus no limitation on the accessible domain of frequencies ω, besides the fact that for very low ω, one needs a lot of memory to store enough data to keep track of the component with the smallest wavelength, of order Λ^{-1}. For strongly dispersive cases, we could reliably access frequencies as low as $10^{-3}T_H$, where $T_H = \kappa/2\pi$ is the Hawking temperature.

On the interval $[x_w, x_f]$, the mode is a sum of the four asymptotic solutions:

$$\varphi^C_\omega(x) = \sum_{j=1}^{4} c_j e^{ik_j x}. \tag{33}$$

Knowing the four roots $k_j(\omega)$, we extract the coefficients c_j by a least-square fitting procedure, tolerating relative errors on the various coefficients of less than 10^{-2}. In practice the

relative precision was usually much better, typically 10^{-5}. We are nevertheless limited by the precision of the numerical integration: the fit fails when the smallest coefficient is smaller than about 10^{-14} times the largest coefficient, which means that the smallest component in Eq. (33) is at the level of the numerical error. This forbids one to approach arbitrarily close to $\omega_{\max}$ since, as we shall see, the occupation number quickly drops when $\omega \to \omega_{\max}$. In the robust regime, this sets an absolute higher bound for the explorable values of ω/κ. Indeed in this regime, $\beta_\omega/\alpha_\omega \simeq e^{-2\pi\omega/\kappa}$, so $\beta_\omega = 10^{-14}\alpha_\omega$ is reached for $\omega/\kappa \simeq 5$, i.e. $\omega/T_H \simeq 30$.

The numerical solution to the wave equation is not normalized, and neither are the asymptotic solutions $e^{ik_j x}$. It does not matter since one only needs the relative norm of each component. Taking into account the normalization of modes when v is constant, see Eq. (14), we define

$$\eta^2 = |c_u|^2\left(\Omega(k^u)\frac{d\omega}{dk^u}\right), \tag{34}$$

for the positive norm, low momentum u component characterized by the root $k^u(\omega)$. In the subluminal case, the Bogoliubov coefficients are thus given by

$$|\beta_\omega|^2 = \frac{|c^u_-|^2}{\eta^2}\Omega(k^u_-)\frac{d\omega}{dk_-}, \tag{35}$$

$$|A_\omega|^2 = \frac{|c^v|^2}{\eta^2}\Omega(k^v)\frac{d\omega}{dk^v}. \tag{36}$$

The same equations hold for superluminal dispersion, with β_ω replaced by β^C_ω, and A_ω by B^C_ω, and with the normalization $\eta_{\rm sup}$ given by

$$\eta^2_{\rm sup} = |c^{u,\rm out}_{-\omega}|^2\left(\Omega(k^{u,\rm out}_{-\omega})\frac{d\omega}{dk^{u,\rm out}_{-\omega}}\right) - |c^{v,\rm out}_{\omega}|^2\left(\Omega(k^{v,\rm out}_{\omega})\frac{d\omega}{dk^{v,\rm out}_{\omega}}\right), \tag{37}$$

since the CJ mode is given by Eq. (29) at late times.

V. RESULTS FOR SUBLUMINAL DISPERSION

A. General properties of the spectra

1. Asymptotic energy flux

The energy flux per $d\omega$ and in units of κ, emitted to the right far from the horizon is equal to (denoting by F the total energy flux)

$$f_\omega = \frac{4\pi^2}{\kappa}\frac{dF}{d\omega} = \frac{\omega}{T_H}|\beta_\omega|^2. \tag{38}$$

The factor $4\pi^2$ is added for convenience, so that $f_\omega \to 1$ for $\omega \to 0$ in the standard case since $T_H = \kappa/2\pi$. This flux is represented in Fig. 9 for $\lambda = \Lambda/\kappa$ fixed to 50, for values of D from 0.02 to 0.2 (left plot), and for D fixed to 0.1 and λ varying from 5 to 130 (right plot).

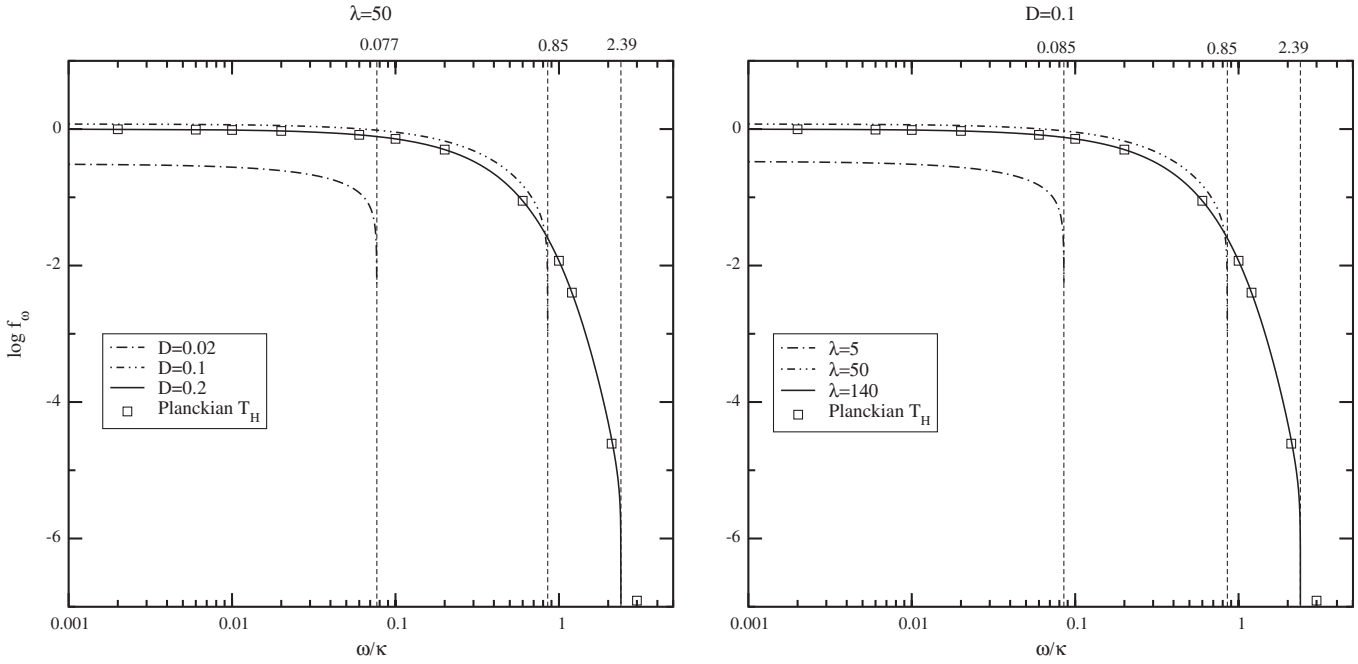

FIG. 9. Logarithm of the energy flux density received far from the horizon. The numbers at the top of the plots give the value of $\omega_{\max}/\kappa$ for each curve. Left plot: λ fixed to 50. $D = 0.02$, 0.1, and 0.2, from left to right. Right plot: D fixed to 0.1. From left to right, $\lambda = 5$, 50, and 130. In both plots, the squares lie along the thermal energy flux with temperature $T_H = \kappa/2\pi$.

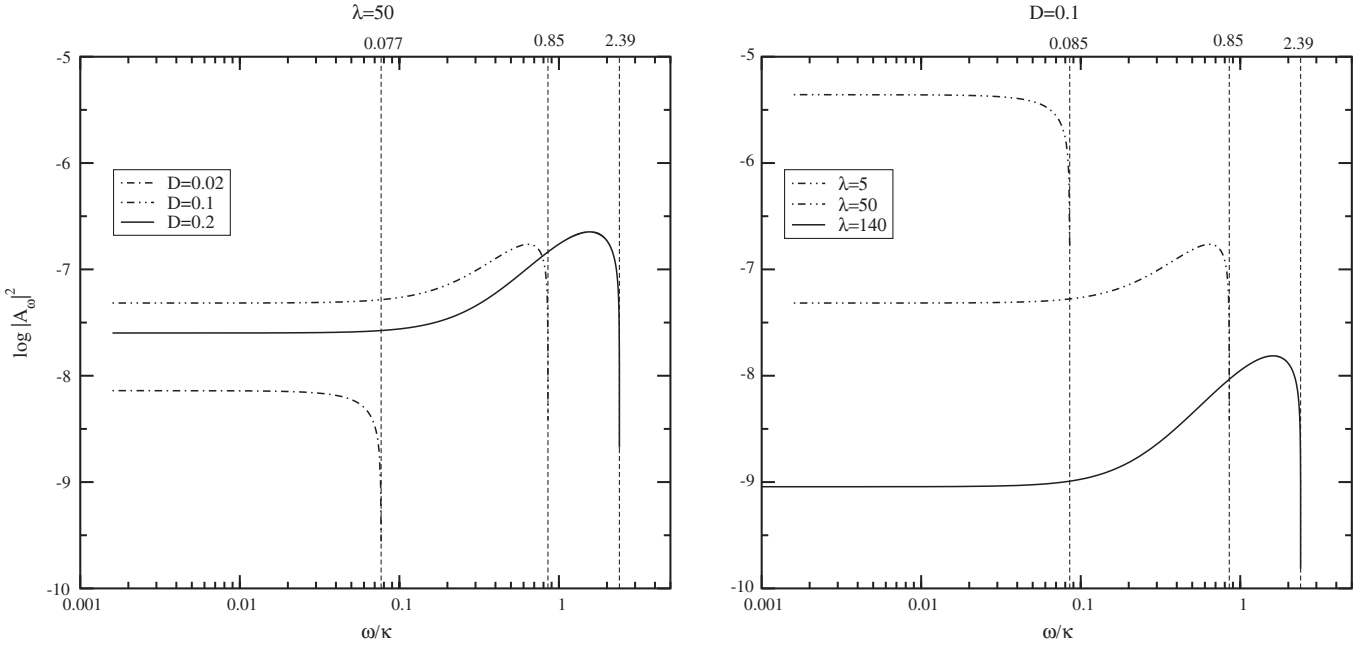

FIG. 10. Logarithm of $|A_\omega|^2$ as a function of ω. In the left plot, λ is fixed to 50, and in the right plot D is fixed to 0.1. The values of the parameters are identical to those in Fig. 9.

All curves exhibit a similar shape. When $\omega \to 0$, f_ω reaches an asymptotic constant value that differs from 1, the dispersionless value, but that becomes very close to it whenever $\omega_{\max} \gg \kappa$. When $\omega_{\max}/\kappa$ is comparable to or smaller than 1, the asymptotic energy flux can be either smaller or greater than the standard one. In addition, its variation with D at fixed λ, or with λ at fixed D, is not monotonic. When ω approaches $\omega_{\max}$, the energy flux quickly drops to zero, in agreement with the theoretical prediction that it vanishes for $\omega > \omega_{\max}$.

2. Mixing between right- and left-moving modes

In Fig. 10, the norm $|A_\omega|^2$ that measures the amount of elastic scattering between right-moving and left-moving modes is represented as a function of ω. The parameters for the left and right plots are the same as in Fig. 9. The curves display a characteristic shape, with a plateau at frequencies much smaller than $\omega_{\max}$, a smooth increase as ω nears $\omega_{\max}$, that gets more pronounced as $\omega_{\max}$ increases. Then, as for the energy flux, there is a sudden falloff when reaching $\omega_{\max}$.

These properties can be qualitatively understood by considering the propagation backward in time of the wave packet of Fig. 7. As long as the evolution is adiabatic, there is no scattering into left movers. The scattering must occur in the relatively well-localized region of space near the turning point, where the WKB approximation breaks down. Its position depends on ω: when $\omega \ll \omega_{\max}$, it is very close to the horizon, and as ω increases, it moves away from the horizon. When it is located in the region where $v(x)$ exits the linear regime with slope κ, $|A_\omega|$ reaches its maximal value. When $\omega \to \omega_{\max}$, the turning point enters into the flat region, and A_ω goes to zero, as expected.

In the right plot of Fig. 10, the height of the low-frequency plateau significantly grows when λ gets smaller. It is therefore interesting to further explore the behavior of $|A_\omega|^2$ for lower values of λ. In Fig. 11, this height is shown as a function of the cutoff frequency $\omega_{\max} = \Lambda f_-(D)$. The growth seen in Fig. 10 saturates when $\omega_{\max} \sim 0.1\kappa$ for

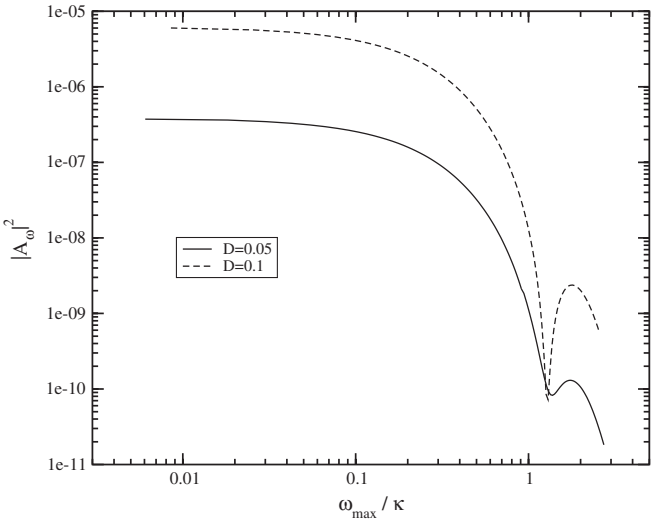

FIG. 11. $|A_\omega|^2$ as a function of $\omega_{\max}$, for $\omega = 0.1 \times \omega_{\max}$, for D equal to 0.05 (solid line) and 0.1 (dashed line). The range in $\omega_{\max}/\kappa$ shown corresponds to values of λ between 0.5 and 150 for $D = 0.1$, and between 1 and 450 for $D = 0.05$.

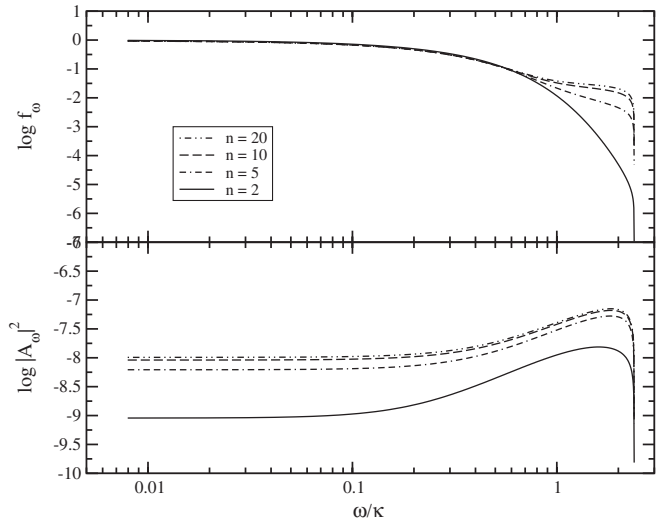

FIG. 12. Upper plot: logarithm of the energy flux density. Lower plot: logarithm of $|A_\omega|^2$. $D = 0.1$ and $\lambda = 140$ in both plots.

both values of D. We also notice that $|A_\omega|^2$ remains smaller than 10^{-5}.

3. Nonadiabatic effects

The power n appearing in Eq. (2) controls the sharpness of the transition between the linearly increasing flow velocity near the horizon and the constant velocity far from it. It thus governs the adiabaticity of the wave propagation at the transition. The qualitative reasoning above suggests that an increase of n should lead to an enhancement of $|A_\omega|^2$ and f_ω short before $\omega_{\max}$. Figure 12 shows that it is indeed the case.

From the upper plot in Fig. 12, we see that the modified f_ω contains a small contribution ($< 3\%$ for $n < 20$) that shows up when the thermal, exponentially decreasing part of f_ω is sufficiently suppressed [10]. Moreover, we see that this contribution is directly related to the nonadiabaticity since it increases with n. Instead, $\omega \ll \kappa/2\pi$ and the low-frequency part of the flux is only slightly affected, as is the rapid falloff for $\omega \to \omega_{\max}$. For $|A_\omega|^2$, a similar enhancement is observed, but it affects all values of ω. This is not surprising, since A_ω is entirely due to nonadiabatic effects.

4. Detailed analysis

In the next sections we successively want to

(i) identify the region of the parameter space (D, λ) where the outgoing flux f_ω is robust, i.e., where its value at $\omega = T_H$ differs little from the standard value $= (e-1)^{-1}$,
(ii) determine, in the robust regime, the behavior of both the leading corrections to the thermal flux, and of the coefficient $|A_\omega|^2$,
(iii) analyze the spectral properties away from the robust regime,
(iv) analyze $\bar{n}^v$ when the growth of the CJ mode is mild,
(v) investigate the properties of the falloff near $\omega_{\max}$,
(vi) analyze the integrated energy flux.

B. Robust regime

We define the robustness of the outgoing radiation by the fact that the energy flux, Eq. (38), differs little when evaluated around $\omega = T_H$, from the thermal flux obtained without dispersion:

$$f^H_\omega = \frac{\omega}{T_H}\frac{1}{\exp(\omega/T_H)-1}. \tag{39}$$

Our aim is twofold. First we wish to characterize the region of the parameter space where f_ω of Eq. (38) hardly differs from f^H_ω. Then we want to determine the scaling properties of the modifications.

To quantitatively study these aspects, we define Δ_H to be the relative difference between the modified and standard energy flux at $\omega = T_H$:

$$\Delta_H = \frac{f_\omega - f^H_\omega}{f^H_\omega}\Big|_{\omega=T_H}. \tag{40}$$

It should be clear that the criterium $\Delta_H \ll 1$ is local in that it is only concerned with what happens for frequencies near the Hawking temperature. The smallness of Δ_H does not imply that $(f - f^H)/f^H$ remains small for all ω, as can be seen from the upper plot in Fig. 12.

1. $\omega_{\max}/\kappa$ is the most relevant parameter

In Fig. 13, Δ_H is represented as a function of $\omega_{\max}/\kappa$ for $\lambda = 8$ and $\lambda = 160$. Although the two values of λ differ by a factor of 20, both curves stay very close to each other

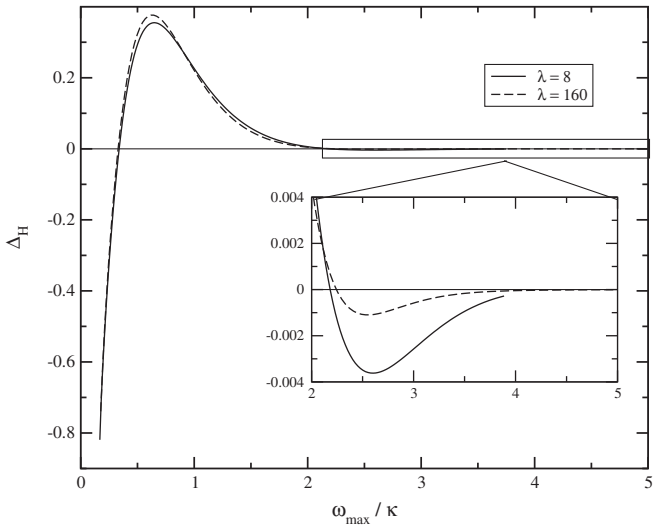

FIG. 13. Δ_H of Eq. (40), as a function of $\omega_{\max}/\kappa$ for $\lambda = 8$ and $\lambda = 160$. In spite of this factor 20, the deviations are extremely similar for all values of $\omega_{\max}$.

even outside the robust regime. This confirms that Λ/κ does not govern the robustness of the radiation. Λ is nevertheless relevant since $\omega_{\max} = \Lambda f(D)$. Hence $\Lambda/\kappa \gg 1$ is not a *sufficient* condition for the robustness, but $\omega_{\max}/\kappa \gg 1$ is.

With more details, starting from the right of Fig. 13 where $\omega_{\max}/\kappa \gg 1$, we find as expected that Δ_H asymptotically vanishes. It stays much smaller than 1 up to $\omega_{\max}/\kappa$ of the order of 2. For smaller values of $\omega_{\max}/\kappa$, Δ_H becomes positive and reaches its maximal value, $\sim 25\%$, for $\omega_{\max}/\kappa \simeq 0.6$. Finally, when $\omega_{\max}/\kappa \to 1/2\pi$ (and thus $\omega_{\max} \to \omega = T_H$), $\Delta_H \to -1$, which means that the flux vanishes, as already discussed.

2. Leading corrections in the robust regime

To determine the scaling properties of the corrections, we have represented in Fig. 14 $\log|\Delta_H|$ as a function of $\log\omega_{\max}/\kappa$ for several fixed values of D. That is, for each curve, λ varies along the curve. The minimum value of $\omega_{\max}$ is such that Δ_H is already in the region where it is small and negative (see Fig. 13).

We see that, whatever the value of D, for $\omega_{\max} > 6\kappa$ ($\log\omega_{\max}/\kappa \gtrsim 0.75$), $\log|\Delta_H|$ is a monotonic linearly decreasing function of $\log\omega_{\max}$. The fact that, for different values of D, the linear regime starts almost at the same $\omega_{\max}$ is a further illustration of its relevance. Had we chosen $\log\lambda$ instead, the linear regime would start at very different abscissa for each value of D.

In the linear regime, the slope is of the order of -4, but slightly varies with D. The precise values of the slopes are -4.42, -4.18, and -4.10 for $D = 0.2$, 0.5, and 0.9, respectively, so the slope gets closer to -4 for a higher D. Surprisingly, a similar behavior is observed for $\log|A_{\omega=T_H}|^2$. The slope is slightly less sensitive to D, as it is equal to -4.05, -4.03, and -4.01, respectively.

The fact that the robust regime, $\Delta_H \ll 1$, is already reached for $\omega_{\max}/\kappa \geq 2$, together with the fact that the slope of $\log\Delta_H$ is of the order of -4 (and not -1 or -2 as one might have expected, and as was found for the power spectrum in inflationary cosmology [29]) demonstrates in a precise and quantitative manner that the thermal properties of Hawking radiation are hardly affected by UV dispersion.

3. Role of the asymptotic velocity $v_+ = -1 + D$

Figure 15 shows the same quantities, but now with a fixed value of λ for each curve, while D varies along the curves. Linear regimes starting at $\omega_{\max}/\kappa \simeq 6$ are again obtained but the slope is of the order of -3 for $\log|\Delta_H|$, whereas it is only -0.2 for $\log|A_{\omega=T_H}|^2$. (More precisely, the slope for $\log|\Delta_H|$ is -2.95 for $\lambda = 50$ and -3.05 for $\lambda = 100$, whereas, for $\log|A_{\omega=T_H}|^2$, it is -0.14 and -0.29, respectively.) D thus affects very differently the pair creation rate and the elastic scattering. This can be understood as follows. Since D fixes the size of the near horizon region where the gradient of v can be approximated by a constant, D governs the amount of redshift suffered by right movers from their turning point to infinity. One thus expects that the deviations from thermality are highly sensitive to D, and this is indeed the case since the log-log power is near to -3. On the contrary, the scattering between right and left movers is not related to the size of the near horizon region. Therefore, one does not expect that $\log|A_{\omega=T_H}|^2$ be strongly dependent on $\log D$. The numerical result ~ -0.2 confirms this expectation.

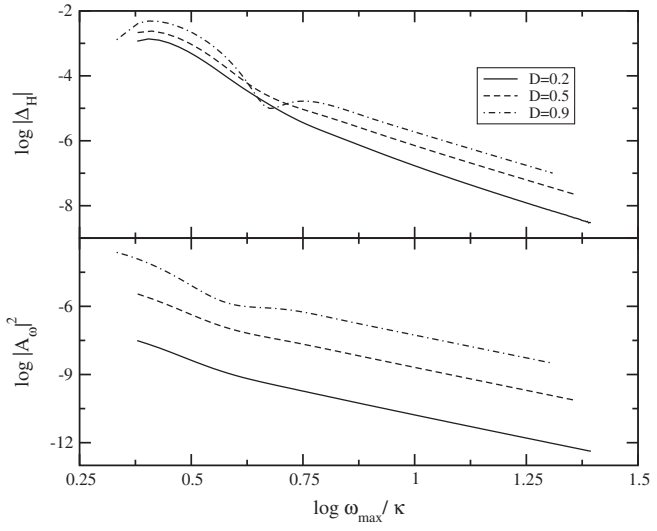

FIG. 14. $\log|\Delta_H|$ and $\log|A_{\omega=T_H}|^2$ as a function of $\log\omega_{\max}/\kappa$ for several values of D. When $\omega_{\max} > 6$, both these quantities become linear, with a slope close to -4.

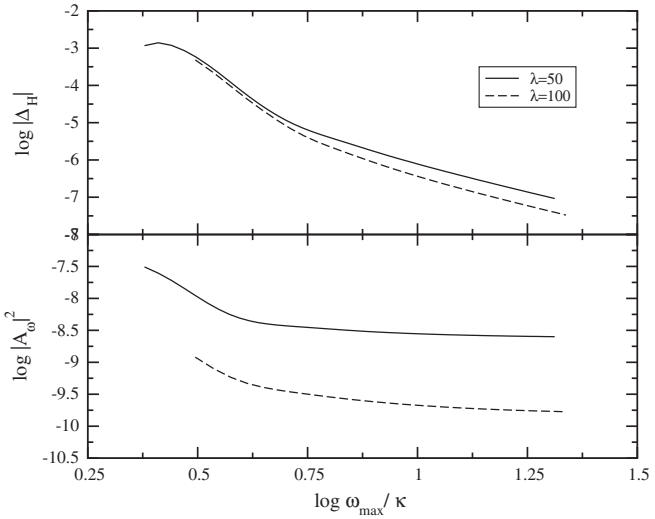

FIG. 15. $\log|\Delta_H|$ and $\log|A_{\omega=T_H}|^2$ as a function of $\log\omega_{\max}/\kappa$ for several values of λ. When $\omega_{\max} > 6$, both these quantities become linear. $\log|\Delta_H|$ has a slope close to 3 for both values of λ, while the slope of $\log|A_{\omega=T_H}|^2$ is very small and is $\simeq 0.14$ for $\lambda = 50$ and $\simeq 0.29$ for $\lambda = 100$.

4. Conclusion and comparison with former work

Since the slopes obtained in Figs. 14 and 15 differ, Δ_H does not scale as a power of $\omega_{\max}/\kappa$ alone. Remembering that $\omega_{\max} = f(D)\Lambda$, we conclude that deep in the robust regime, the first corrections to the thermal spectrum can be written as

$$\Delta_H = -g(D, \Lambda/\kappa) \times \left(\frac{\kappa}{\omega_{\max}}\right)^3 \times \left(\frac{\kappa}{\Lambda}\right), \qquad (41)$$

where $g(D, \Lambda/\kappa)$ is positive and varies only slowly with the parameters.

This result differs from what was reported in [10]. In that paper, D was fixed to 0.5, and the scaling of Δ_H with respect to λ was reported to be characterized by a power close to 1. However, there is no real contradiction as can be understood from Fig. 16, where the same quantities are represented as in the previous figures, for $D = 0.5$, and several values of n. We see that, as n increases, the superimposed oscillations become more pronounced and last until higher values of $\omega_{\max}/\kappa$. In fact, we see two regimes. When n is smaller than about 4, the linear regime with a slope close to -4 remains. Instead, for $n = 5$ the nonadiabatic effects dominate and the linear regime is lost. In this sense, the low values of n correspond to a *superrobust* regime, with well-defined first corrections to thermality and with a clear scaling in the parameters. In [10], the scaling was estimated for a kinked velocity profile, which corresponds to the limit $n \to \infty$. In this limit, the nonadiabatic effects largely dominate and this probably explains why the authors missed the scaling as $(\lambda)^{-4}$.

It is also interesting to note that the behavior of $\log|A_{\omega=T_H}|^2$ is more robust to changes in n since the linear regime exists longer, and the slope and intercept are not significantly modified.

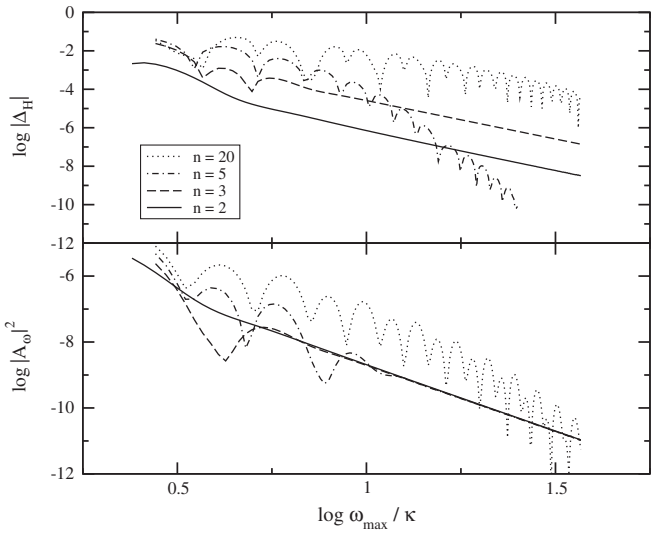

FIG. 16. $\log|\Delta_H|$ and $\log|A_{\omega=T_H}|^2$ as a function of $\log\omega_{\max}/\kappa$ for $D = 0.5$ and different values of n.

C. Black hole radiation outside the robust regime

In the strongly dispersive regime, if one can expect large deviations, i.e. $O(1)$, with respect to the standard flux of Eq. (39), one has *a priori* no idea of what the properties of these deviations could be, nor how generic they are. Moreover, we do not think that they can be computed analytically. However, with our code we were able to compute them when $\omega_{\max}/\kappa \lesssim 1$, and, to our surprise, we found that thermality is preserved in the low-frequency part of the spectrum. In addition, because of the smallness of $\omega_{\max}/\kappa$, the growth of the CJ mode is moderate, and this allowed us to compute the observable $\bar{n}^v_\omega$ which we could not have access to in the robust regime.

1. Right-moving flux $\bar{n}_\omega$

To characterize the modified properties of the flux we found *a posteriori* that it is convenient to use the effective temperature T_ω defined by

$$\bar{n}_\omega = |\beta_\omega|^2 = \frac{1}{\exp(\omega/T_\omega) - 1}. \qquad (42)$$

In Fig. 17, T_ω/T_H is represented as a function of $\omega/\omega_{\max}$ for $D = 0.1$ and different values of λ. Besides the expected quick drop of the power when $\omega \to \omega_{\max}$, two remarkable features emerge: first, for all values of $\omega_{\max}$, T_ω is nearly constant for $\omega < \omega_{\max}/10$. Second, the asymptotic temperature $T_0 = T_{\omega\to 0}$ strongly differs from T_H when $\omega_{\max}/\kappa$ is small.

These two properties suggest studying two types of corrections: a (global) temperature shift, characterized by $T_0 - T_H$, and a deviation from thermality, characterized by the running of T_ω in ω. To sort out these two effects, we fit

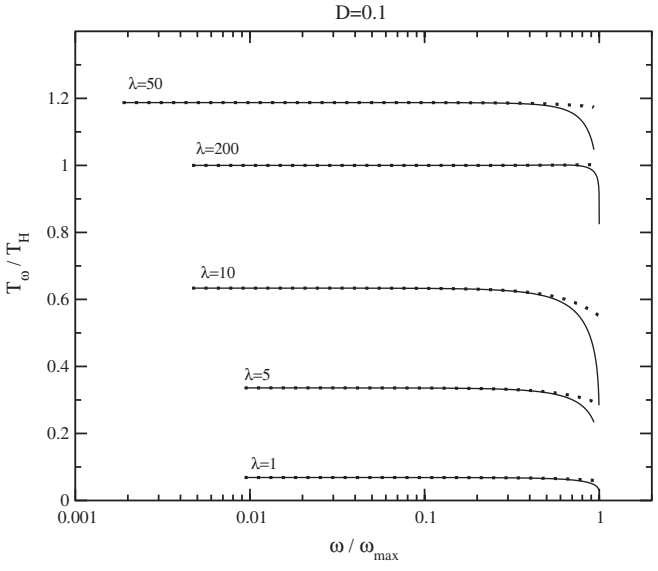

FIG. 17. Effective temperature T_ω as a function of $\omega/\omega_{\max}$, for $D = 0.1$ and various values of λ. The dots show the fits obtained using the ansatz Eq. (43).

TABLE I. Fitting parameters for the low frequency part of the effective temperature $T(\omega)$. Notations are defined in Eq. (43). D is fixed to 0.1.

λ	$\omega_{\max}/\kappa$	T_0/T_H	R	s
200	3.4	0.999 87	3.0×10^{-3}	2.05
140	2.4	0.999 5	-5.5×10^{-3}	1.96
50	0.85	1.187	-1.8×10^{-2}	2.06
10	0.17	0.633 7	-8.3×10^{-2}	2.01
5	0.085	0.336 0	-4.8×10^{-2}	2.01
1	0.017	0.068 57	-1.0×10^{-2}	2.01

the curves with

$$T_\omega/T_H = T_0/T_H + R\left(\frac{\omega}{\omega_{\max}}\right)^s. \tag{43}$$

The fits are shown as dotted lines in Fig. 17. They coincide perfectly with the curves at low frequencies and start to depart only around $\omega = \omega_{\max}/2$. The fit parameters are found to be those of Table I. As expected, when $\omega_{\max}/\kappa$ is large, T_0 becomes very close to T_H. In all cases, the power s is close to 2, and the coefficient R is much smaller than 1.

We are now in a position to determine to what extent the modified spectrum can be considered thermal. To this end, let us compare the temperature shift

$$\Delta_0 = \frac{T_H - T_0}{T_H}, \tag{44}$$

with the running of T_ω, that we characterize by

$$\Delta_{T_0} = \frac{T_0 - T_{\omega=T_0}}{T_0}. \tag{45}$$

($T_{\omega=T_0}$ is the value given by the true curve, not the fit.) We find the parameters as those of Table II. When $\omega_{\max}/\kappa$ is large, these numbers make more precise the statement made before that we recover a Planck spectrum with the standard temperature, truncated when $\omega \to \omega_{\max}$. Indeed, both the temperature shift and the running in ω are extremely small.

When $\omega_{\max}/\kappa$ becomes small enough, as is the case for values $\lambda < 50$ in Table I, the departure from the standard flux becomes significant. Nevertheless, there is a clear ordering between the temperature shift and the running, the former being always much bigger than the latter. Thus, as a first approximation, the modified spectrum can be seen as a Planckian spectrum with a nonstandard temperature, and truncated for $\omega \to \omega_{\max}$, and this is even far away from the robust regime.

TABLE II. Shift Δ_0 and running Δ_{T_0} of the effective temperature $T(\omega)$. D is fixed to 0.1.

$\omega_{\max}/\kappa$	Δ_0	Δ_{T_0}
3.4	1.3×10^{-4}	<num. prec.
2.4	5.4×10^{-4}	3.1×10^{-5}
0.85	-0.19	7.8×10^{-4}
0.17	0.37	0.061
0.085	0.66	0.77
0.017	0.93	0.083

To complete our analysis, in Fig. 18, T_ω is shown for several couples (λ, D), such that $\omega_{\max}/\kappa$ remain fixed to 0.8. T_0 slightly varies ($\sim 3\%$) from one curve to another, and is thus not controlled only by $\omega_{\max}$. However, the relative variations of T_0 are much smaller than the changes in λ. This shows what we had announced, namely, that the modification of the spectra is essentially governed by $\omega_{\max}/\kappa$ and almost degenerate along the contours of constant $\omega_{\max}/\kappa$ in the (λ, D) plane. In fact, when λ becomes high, T_0 saturates at a maximum value ($\neq T_H$) which is truly fixed by $\omega_{\max}/\kappa$ alone.

In the lower plot of Fig. 18, the effect of n on T_ω is investigated, for $\omega_{\max}/\kappa = 0.8$ and $\lambda = 10$. The higher n, the higher T_0. The value of T_0 saturates at a maximum value when n becomes high. We have also checked that the dependence of T_0 on n is smaller when λ is higher, as could be expected by looking at Fig. 12.

To conclude this section, we point out that the fact that the temperature shift of Eq. (44) is much larger than the running governed by Δ_{T_0} of Eq. (45) for the entire class of metrics we considered severely limits the possibility, raised in [27], that "the ω dependence of the Hawking temperature can be explained by the fact that high-energy wave packets have a different group velocity than those at low energy and hence the various modes 'see' different horizons and thus other values for the surface gravity." Were this picture valid, the shift Δ_0 would vanish since low-frequency wave packets travel at the speed $c = 1$ and thus see the standard surface gravity $\kappa = \partial_x v|_{x=0}$.

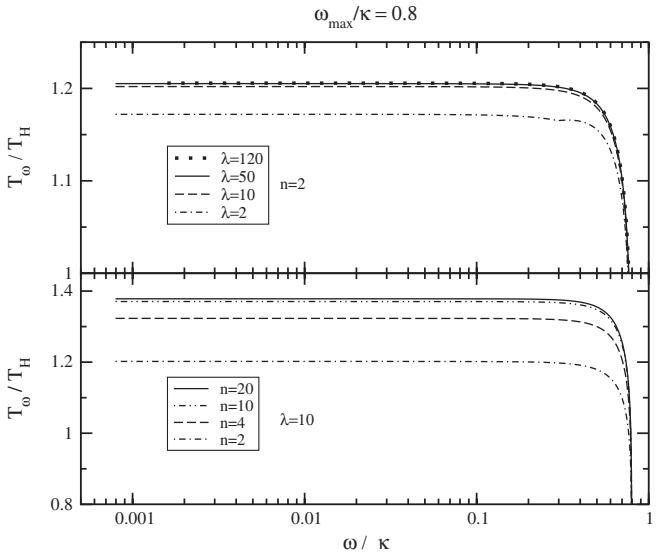

FIG. 18. Effective temperature T_ω as a function of ω/κ, for $\omega_{\max}/\kappa = 0.8$. Upper plot: n fixed to 2, λ varies; lower plot: $\lambda = 10$, n varies.

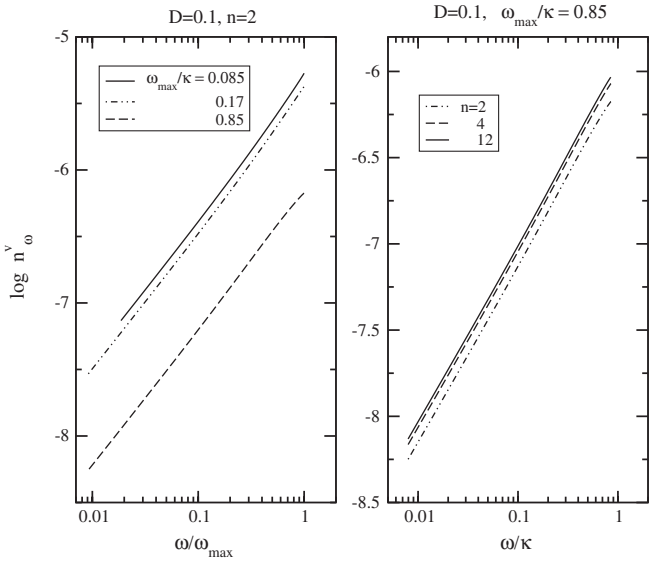

FIG. 19. Left plot: $\bar{n}^{\upsilon}_{\omega}$ as a function of $\omega/\omega_{\max}$ for various values of $\omega_{\max}/\kappa$, and with $D = 0.1$ and $n = 2$. Right plot: $\bar{n}^{\upsilon}_{\omega}$ as a function of ω/κ for various values of n, and with $\omega_{\max}/\kappa = 0.85$, $D = 0.1$.

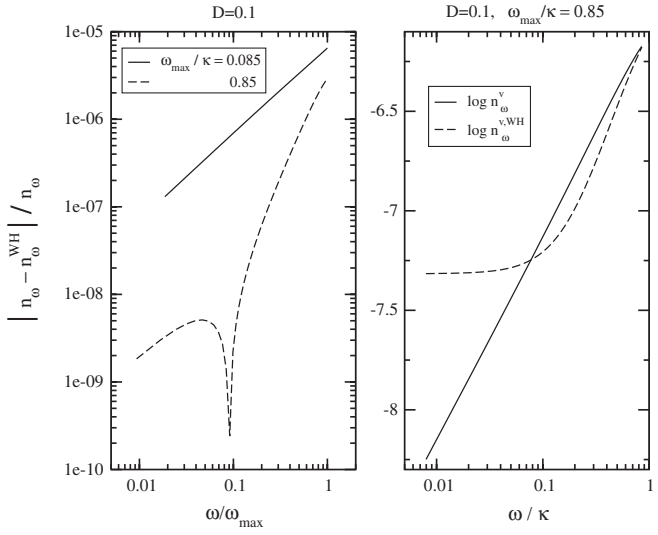

FIG. 20. Left plot: relative difference between $\bar{n}^{\mathrm{WH}}_{\omega}$ and $\bar{n}_{\omega}$ as a function of $\omega/\omega_{\max}$, for $\omega_{\max}/\kappa = 0.085$ and 0.85, and $D = 0.1$. Right plot: $\bar{n}^{\upsilon}_{\omega}$ and $\bar{n}^{\upsilon,\mathrm{WH}}_{\omega}$ as a function of ω/κ for $\omega_{\max}/\kappa = 0.85$ and $D = 0.1$.

2. Left-moving flux $\bar{n}^{\upsilon}_{\omega}$

When $\omega_{\max}/\kappa \lesssim 1.5$, the CJ mode grows only slowly toward the horizon. It is thus possible to compute the other modes.3 With three independent modes at hand, we can compute the nine coefficients of the Bogoliubov transformation. Here, we present (for the first time in the literature) quantitative results concerning the production of left-moving particles, governed by $\bar{n}^{\upsilon}_{\omega} = |\tilde{B}_{\omega}|^2$. It is represented in the left panel of Fig. 19 as a function of $\omega/\omega_{\max}$ for D fixed to 0.1 and for three values of $\omega_{\max}/\kappa$, namely, 0.085, 0.17, and 0.85. We note that $\bar{n}^{\upsilon}_{\omega}$ is, to a good approximation, linear in $\omega/\omega_{\max}$. Hence it does not go to zero when $\omega \to \omega_{\max}$, in agreement with the fact that both $\varphi^{u,\mathrm{out}}_{-\omega}$ and $\varphi^{\upsilon,\mathrm{out}}_{\omega}$, and thus the coefficient $\tilde{B}_{\omega}$ in Eq. (23), remain well defined above $\omega_{\max}$ in the subluminal case.

In the right panel of Fig. 19 the influence of the nonadiabatic parameter n is investigated. As expected, the production of left movers is more important when n is higher. However, the dependence on n is weak and saturates when n becomes high.

3. WH vs BH fluxes

Having access to the full Bogoliubov transformation of Eq. (23), we can also compute the difference between the fluxes emitted by WH and BH. From the algebraic treatment, we can assert [using the unitarity of Eq. (23)] that the difference of fluxes obeys

$$\bar{n}^{\mathrm{WH}}_{\omega} - \bar{n}_{\omega} = -(\bar{n}^{\upsilon,\mathrm{WH}}_{\omega} - \bar{n}^{\upsilon}_{\omega}). \tag{46}$$

However, to actually compute this difference, a numerical treatment is required. The relative difference $(\bar{n}^{\mathrm{WH}}_{\omega} - \bar{n}_{\omega})/\bar{n}_{\omega}$ is represented in Fig. 20 for $D = 0.1$ and $\omega_{\max}/\kappa = 0.085$ and 0.85. This difference stays below 10^{-5}. Moreover it decreases when $\omega_{\max}/\kappa$ increases, i.e. when going toward the robust regime, as one expected since it must vanish when the u-υ mixing itself vanishes.

For the larger value of $\omega_{\max}/\kappa$ one can see that the relative difference changes sign. This can be understood from Eq. (46) and Fig. 19, where we have seen that $\bar{n}^{\upsilon}_{\omega}$ is proportional to ω while $\bar{n}^{\upsilon,\mathrm{WH}}_{\omega} = |B_{\omega}|^2$, shown in the right plot in Fig. 20, is constant at low frequencies. Thus one always has $\bar{n}^{\mathrm{WH}}_{\omega} > \bar{n}_{\omega}$ at low enough frequencies. Notice also that contrary to the u occupation numbers, $\bar{n}^{\mathrm{WH}}_{\omega}$ and $\bar{n}_{\omega}$, neither of the $\bar{n}^{\upsilon}_{\omega}$'s vanishes at $\omega_{\max}$, but they become equal, ensuring that at all frequencies Eq. (46) is satisfied.

Finally we notice that the relative difference does not diverge for $\omega \to \omega_{\max}$, which implies that $\bar{n}^{\mathrm{WH}}_{\omega}$ goes to zero near $\omega_{\max}$ as quickly as $\bar{n}_{\omega}$.

D. Near $\omega_{\max}$ region

To complete our study of the spectrum, we investigate the quick falloff near $\omega_{\max}$. We find that, both for the energy flux and for $|A_{\omega}|^2$, the falloff presents a universal behavior (for the class of velocity profiles considered), independent of λ, D, and n. Indeed we find that

$$f_{\omega} = h_F(D, \lambda) \times \sqrt{\frac{\Delta\omega}{\omega_{\max}}}, \tag{47}$$

where $\Delta\omega = \omega_{\max} - \omega$, and similarly for $|A_{\omega}|^2$, with h_F replaced by a different function of D and λ, h_A.

Figure 21 shows $\log f_{\omega}$ and $\log|A_{\omega}|^2$ versus $\log\Delta\omega/\omega_{\max}$, near $\omega = \omega_{\max}$. λ is fixed to 50 and each

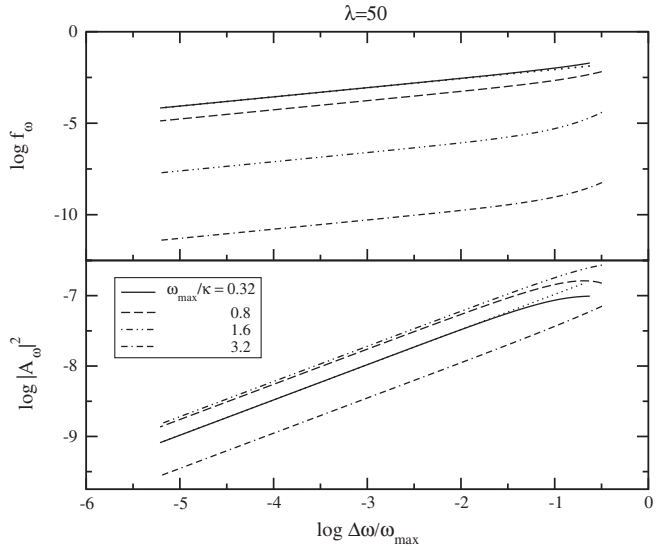

FIG. 21. $\log f_\omega$ (upper plot) and $\log|A_\omega|^2$ (lower plot) as functions of $\log\Delta\omega/\omega_{\max}$ for $\lambda = 50$ and several values of $\omega_{\max}/\kappa$. The legend applies to both plots. The dotted line has a slope exactly equal to 0.5 and fits perfectly the $\omega_{\max} = 2$ curves. All curves have the same slope in their linear region.

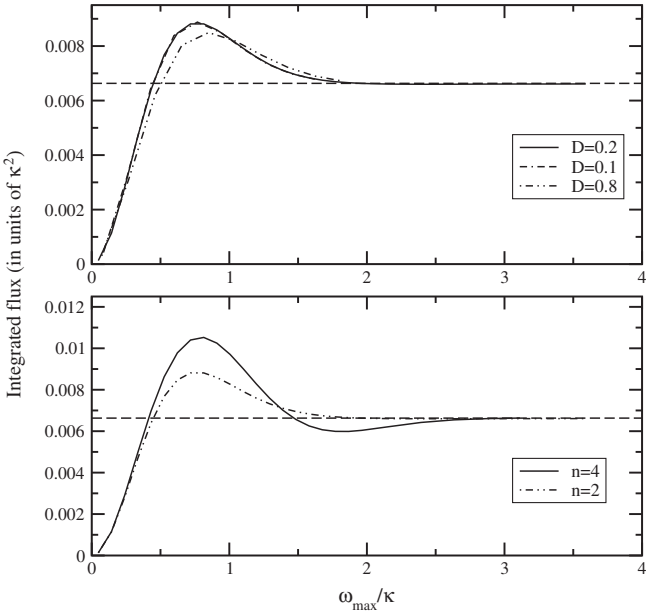

FIG. 22. Integrated flux in units of κ^2, as a function of $\omega_{\max}/\kappa$. Upper plot: n fixed to 2, several values of D. Lower plot: D fixed to 0.2, several values of n. The horizontal line is the standard value ($= 1/48\pi$) of the integrated flux obtained using the dispersionless theory.

curve corresponds to a different value of $\omega_{\max}$. Both quantities are linear when ω is close enough to $\omega_{\max}$, with a slope precisely equal to 0.5, independently of the value of $\omega_{\max}$. We verified that this behavior is also independent of λ. Finally we have also verified that the value of n, which strongly affects the behavior of the spectrum near $\omega_{\max}$, as can be seen from Fig. 12, does not affect Eq. (47).

E. Integrated energy flux

In this section, we present the main features of the integrated energy flux obtained by integrating over ω the differential flux f_ω. It is computed as a Riemann sum and depends on D, λ, and n. The sum is computed from $\omega/\kappa = 10^{-3}$, where the asymptotic value of f_ω is reached to a good precision, until $\omega/\kappa = \omega_{\max}/\kappa - 10^{-5}$. The step in ω/κ is 0.01, so that the relative variation between two successive points is small. Under these conditions, the Riemann sum gives a very good estimate of the integral.

The upper plot in Fig. 22 shows the integrated flux as a function of $\omega_{\max}/\kappa$ for several values of D, and n fixed to 2. Like T_0 and Δ_H, the integrated flux converges rapidly to its standard value for $\omega_{\max}/\kappa > 2$, even though the flux density f_ω differs from the standard one for high frequencies. In other words, the nonlocal robustness criterium, that the integrated flux be close to standard, agrees with the local one defined in Sec. V B. This is because the exponential tail of the standard f_ω contributes only marginally to the integral, so that the cutoff at $\omega_{\max}$ in the modified flux does not cause noticeable differences in the integrated flux.

The lower plot of Fig. 22 shows that when n increases, the amplitude of the oscillations in the integrated flux is more important, and they last until higher values of $\omega_{\max}$. This reflects the fact that the nonthermal part of f_ω yields a non-negligible contribution to the integrated flux and can be understood looking at Fig. 12 where the enhancement of the high-frequency part of the spectrum through nonadiabatic effects was shown.

VI. RESULTS FOR SUPERLUMINAL DISPERSION

A. General properties of the spectra

1. Smallness of u-v mixing

As can be seen from Eq. (30), $|\beta^C_\omega|^2$ is not exactly equal to $\bar{n}_\omega$. In the following we make the approximation $\bar{n}_\omega \simeq |\beta^C_\omega|^2$, whose validity requires $|A_\omega|^2 \ll 1$. To justify this, we first show that the inequality is indeed verified everywhere we can compute $|A_\omega|^2$. $|A_\omega|^2$ is shown in Fig. 23 for different values of $\omega_{\max}$. At fixed D, on the left plot, it strongly decreases when $\omega_{\max}/\kappa$ increases. For instance, it remains smaller than 10^{-7} for $\omega_{\max}/\kappa = 1.39$. At fixed λ, on the right plot, it becomes monotonically decreasing only for high enough values of D, but stays always smaller than 10^{-6} for $\lambda = 50$. These results strongly suggest that it must be even smaller in the region of the parameter space where it is inaccessible to our code. As we shall see in the next section, the important result is that it is always much smaller than both the modifications with respect to the standard flux, and the relative difference between the super- and subluminal fluxes. The approximation $|\beta^C_\omega|^2 \simeq \bar{n}_\omega$ thus induces only a negligible error.

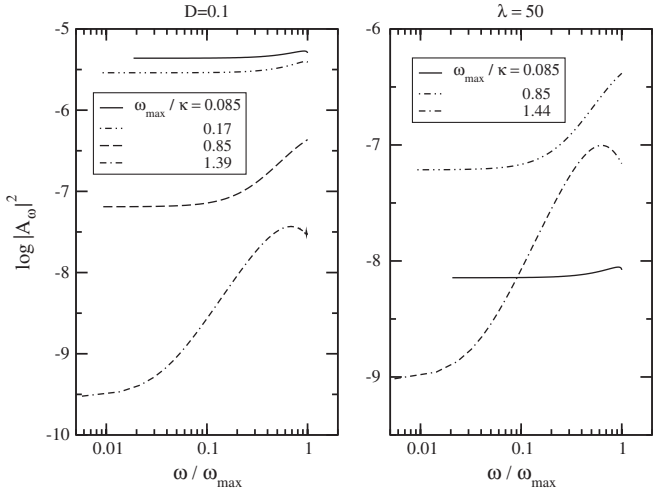

FIG. 23. The u-v mixing coefficient $|A_\omega|^2$ governing the difference between $|\beta^C_\omega|^2$ and $|\beta_\omega|^2$, see Eq. (30), as a function of ω, for various values of $\omega_{\max}$. Left plot: D fixed to 0.1. Right plot: λ fixed to 50.

Note also that, unlike what was found in Figs. 10 and 12, $|A_\omega|^2$ does not vanish for $\omega \to \omega_{\max}$ in the superluminal case. This is because $\varphi^{u,\text{out}}_\omega$ and $\varphi^{v,\text{out}}_\omega$ remain well defined above $\omega_{\max}$ so that, at $\omega_{\max}$, A_ω smoothly connects to R_ω of Eq. (22).

2. Comparison between super- and subluminal dispersion

In analogy with Eq. (38), we define the flux

$$f^C_\omega = \frac{2\pi\omega}{\kappa}|\beta^C_\omega|^2. \tag{48}$$

To our surprise, we found that f^C_ω is extremely close to f^{sub}_ω of Eq. (38) when working with the same background geometry (i.e. the same value of D and n) and the same value of $\omega_{\max}$. This unexpected similarity shows once more that $\omega_{\max}$ is the relevant parameter for characterizing the departure from the dispersionless case.

Although f^{sub}_ω of Eq. (38) and f^C_ω belong to two different models, it does make sense to study their difference when one works with the same velocity profile $v(x)$, so as to have the same behavior in the dispersionless regime, and the same value of $\omega_{\max}$. (Under these conditions, the two values of Λ cannot be exactly the same, but are close to one another.) In Fig. 24, the relative difference $(f^C_\omega - f^{\text{sub}}_\omega)/f^{\text{sub}}_\omega$ is represented versus $\omega/\omega_{\max}$ for a fixed $D = 0.1$, and a series of increasing values of $\omega_{\max}$. The chosen values of $\omega_{\max}/\kappa$ correspond to $\lambda = 5$, 50, and 140, respectively, for subluminal dispersion, and slightly different values for superluminal dispersion, tuned to get the same $\omega_{\max}/\kappa$. The relative differences are of about 5% when $\omega_{\max}/\kappa = 0.085$, but are extremely small for $\omega_{\max}/\kappa = 0.85$ and $\omega_{\max}/\kappa = 2.39$, except in a thin region near $\omega_{\max}$.

The right plot in Fig. 24 also represents the relative difference between f^C_ω and the standard energy flux.

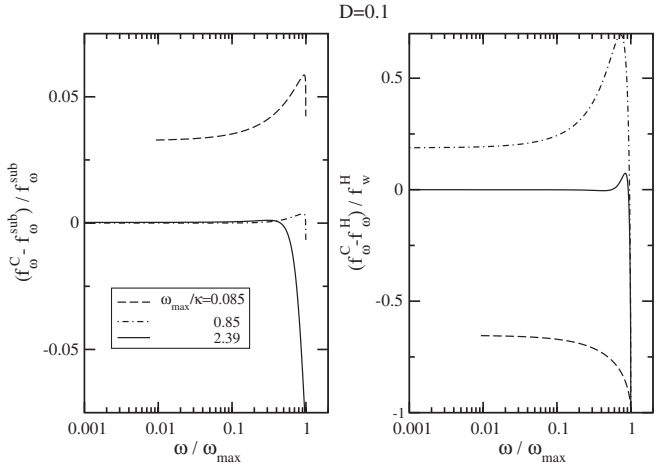

FIG. 24. Left plot: relative difference of the energy flux densities with superluminal and subluminal dispersion, as a function of ω/κ. The background geometry is fixed, with $D = 0.1$ and $n = 2$. $\omega_{\max}/\kappa$ varies from 0.085 to 2.39. Right plot: relative difference between f^C_ω and the standard energy flux f^H_ω, for the same set of parameters.

When the spectrum is not robust, as is the case for $\omega_{\max}/\kappa < 1$, the modifications with respect to the standard spectrum are much larger than the differences between the super- and subluminal spectra. In this sense, the modifications are controlled essentially by the value of $\omega_{\max}/\kappa$, and seem to depend only marginally on the precise nature of the dispersion relation.

This point can be made more precise with the help of Fig. 25, where the same quantities as in Fig. 24 are represented, but this time with $\omega_{\max}/\kappa$ held fixed, equal to 0.1, and a varying D. The values of λ corresponding to $D = 0.02$, 0.05, and 0.3 are 64.84, 16.36, and 1.09, respectively,

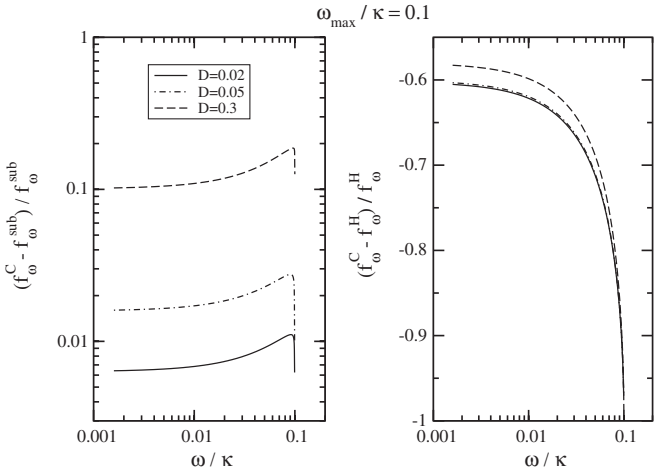

FIG. 25. Left plot: relative difference of the energy flux densities with superluminal and subluminal dispersion. $\omega_{\max}/\kappa$ fixed to 0.1; D varies from 0.02 to 0.3. Right plot: relative difference between f^C_ω and the standard energy flux f^H_ω, for the same set of parameters.

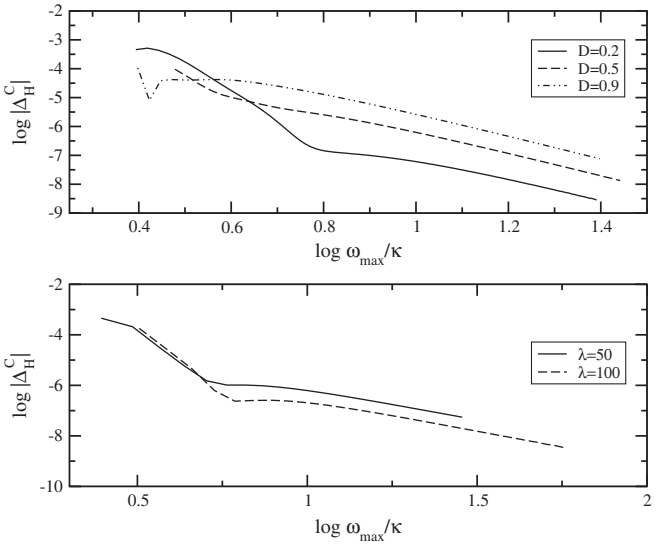

FIG. 26. Scaling of Δ_H^C with $\omega_{\max}/\kappa$, for fixed D (upper plot) and for fixed λ (lower plot).

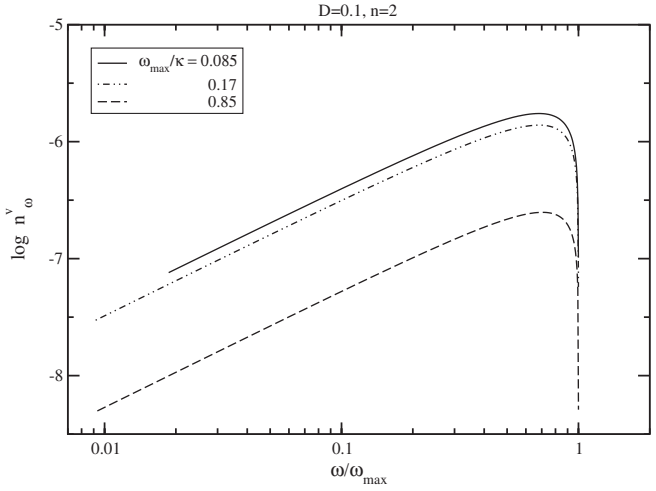

FIG. 27. $\bar{n}_\omega^\upsilon$ as a function of $\omega/\omega_{\max}$, for $\omega_{\max}/\kappa$ from 0.085 to 0.85, with D fixed to 0.1.

for subluminal dispersion (and of course slightly different for superluminal dispersion). From the right plot in that figure, it is clear that for this fixed value of $\omega_{\max}/\kappa$, large variations of (D, λ) cause only small variations in the corrections to the standard flux. In fact, as expected, the greater the scale separation between Λ and κ, the more precise the statement that essentially only $\omega_{\max}/\kappa$ matters and not the precise nature of the dispersion relation. This is illustrated by the left plot, where we see that as D decreases (and thus as λ increases to maintain $\omega_{\max}/\kappa$ fixed), the relative difference between f_ω^C and $f_\omega^{\rm sub}$ becomes smaller and smaller.

The smallness of the differences in the energy flux between sub- and superluminal dispersion teaches us several lessons. First, as soon as $\omega_{\max}/\kappa \gtrsim 1$, the quantitative agreement, to a fraction of a percent, of the superluminal results with the subluminal ones (at least for frequencies not too close to $\omega_{\max}$) means that the global properties for a given $\omega_{\max}$ of the spectra for sub- and superluminal dispersion, such as the modified temperature, the running of the temperature, and the total energy flux, are the same to a very good approximation. Thus, we do not repeat in the case of superluminal dispersion the studies performed in Secs. V C and V E, since the results are qualitatively and quantitatively the same. Secondly, the robustness criterium and the range of robustness are the same for both types of dispersion. That is, the radiation is robust for $\omega_{\max}/\kappa > 2$ in both cases.

B. First corrections to Hawking radiation in the robust regime

The above agreement between $f_\omega^{\rm sub}$ and f_ω^C suggests that the scalings of the leading corrections with respect to the standard spectrum are also similar for sub- and superluminal dispersions. This point is investigated in Fig. 26, where the logarithm of

$$\Delta_H^C = (f_\omega^C - f_\omega^H)/f_\omega^H|_{\omega=T_H} \tag{49}$$

is represented versus the logarithm of $\omega_{\max}/\kappa$ for several fixed values of D and λ.

Like in the subluminal case, a ''superrobust'' regime is reached for $\omega_{\max}/\kappa \gtrsim 6$. The slopes differ also slightly from the subluminal case. In the upper plot, we find -3.46, -3.79, and -3.88 for $D = 0.2$, $D = 0.5$, and $D = 0.9$, respectively. In the lower plot, the slopes are -2.42 and -2.48 for $\lambda = 50$ and 100, respectively. The scaling in λ, at fixed D, of the first corrections is still with a power close to -4 in the superluminal case, while the scaling in $f_+(D)$ at fixed λ is with a power between 2 and 3. It is also worth mentioning that Δ_H^C is negative in the superrobust regime, as was $\Delta_H^{\rm sub}$. This is opposed to the first corrections to the inflationary spectra that have different signs for sub- and superluminal dispersions (see [29]).

C. Production of left movers

Figure 27 shows the occupation number $\bar{n}_\omega^\upsilon$ for superluminal dispersion for $D = 0.1$ and the same values of $\omega_{\max}/\kappa$ as in Fig. 19. As in the subluminal case, it decreases when $\omega_{\max}/\kappa$ increases. It is proportional to ω for $\omega \lesssim 0.1 \times \omega_{\max}$, but contrary to the subluminal case, it goes to zero when ω approaches $\omega_{\max}$. This is as expected since the negative frequency partners of these υ quanta exist only for $\omega < \omega_{\max}$.

D. Near $\omega_{\max}$ region

Finally, we have investigated the behavior of the fluxes near the maximum frequency. We find that both n_ω^υ and f_ω^C decrease like $(\omega_{\max} - \omega)^{1/2}$ near $\omega_{\max}$, as $f_\omega^{\rm sub}$ and $|A_\omega^{\rm sub}|^2$ did [see Eq. (47)].

E. Comparison with Ref. [34]

In Ref. [34], when considering a time-dependent collapsing background metric, the authors reached the conclusion that Hawking radiation is no longer stationary when dealing with a quartic superluminal dispersion relation. We believe this conclusion is not due to the time-dependent character of the geometry, but is rather due to the use of a geometric optic approximation, in Eq. (4.14), in a regime where it is not valid, as indicated by the numerical results of [21]. However, a detailed calculation of the fluxes remains to be done.

VII. CONCLUSIONS

We have studied the properties of the fluxes emitted by acoustic black holes when taking into account the effects induced by sub- and superluminal dispersion relations. We focused on one-dimensional stationary flows which possess two asymptotic regions. In this case, unlike what is found for gravitational black holes, the fluxes emitted on both sides of the horizon are well-defined observables.

At the theoretical level, we showed that the dimensionality of the space of asymptotically bounded stationary modes is three, and that this space is complete. This guarantees that the 3×3 Bogoliubov transformation of Eq. (23) relating in and out modes is unitary. It reduces to a 2×2 matrix only if left- and right-moving modes completely decouple, which is a degenerate case, probably never found in condensed matter systems. We then showed that because of dispersion, a critical frequency $\omega_{\max}$ exists above which no radiation is emitted, and the 3×3 transformation simplifies into Eq. (22). This frequency depends both on the UV scale Λ characterizing the dispersion, and on the asymptotic properties of the background geometry. Because of the dispersion as well, the fluxes emitted by white holes are well defined and regular. Moreover we established how they are related to those of the corresponding black hole; see Eq. (26) and Fig. 20.

We have computed numerically the fluxes in the case of quartic sub- and superluminal dispersions. The main result of our analysis is the following. The deviations with respect to the standard dispersionless fluxes are highly degenerate along the lines of constant frequency $\omega_{\max}$, see Figs. 13 and 18, and, as a corollary, are essentially governed by $\omega_{\max}/\kappa$.

Our second result concerns the characterization of the range of the robustness, i.e. the range of the parameters within which the deviations are small. We first found that for $\omega_{\max}/\kappa > 6$, there is a superrobust regime in which the leading deviations rapidly decrease as a power law in $\kappa/\omega_{\max}$, where the power is equal to 3 or 4 depending on which parameter is held fixed; see Figs. 14 and 15. We also showed that for $\omega_{\max}/\kappa > 2$, the deviations are already smaller than a percent.

Our third important result concerns the absence of a significant running of the effective temperature, Eq. (42), even when leaving the robust regime. The low-frequency part of the fluxes, i.e. $\omega < 0.1 \times \omega_{\max}$, is indeed well characterized by a common temperature that significantly differs, for $\omega_{\max}/\kappa < 1$, from the standard temperature $\kappa/2\pi$ but that hardly changes with ω; see Table I. This implies that the effective temperature T_ω is probably not related in a universal manner to the gradient of the flow velocity v evaluated at some ω-dependent horizon, in agreement with the remarks made in [10].

Fourth, we have also presented quantitative results concerning the production of v quanta in the domain $\omega_{\max}/\kappa \lesssim 1$. We found numerically that $\bar{n}^v_\omega$ is proportional to ω at low frequencies; see Figs. 19 and 27.

Finally we showed in Sec. VI that the deviations obtained using sub- and superluminal dispersion are unexpectedly similar when using theories having the same $\omega_{\max}$. This means that the deviations with respect to the standard fluxes obtained with each theory are much larger than the difference between these deviations, typically by a factor of more than 10; see Fig. 25. However, these conclusions are probably related to the fact that our velocity profiles are symmetrical with respect to the horizon and possess two asymptotic regions. When considering profiles describing gravitational black holes, we expect that the deviations due to sub- and superluminal dispersion will differ more significantly. We also expect our results for subluminal dispersion to apply to gravitational black holes because the CJ modes essentially live in the outside region, as can be seen in Fig. 7.

ACKNOWLEDGMENTS

We would like to thank the organizers and the participants of the workshop "Towards the Observation of Hawking Radiation in Condensed Matter Systems" (http://www.uv.es/workshopEHR/) held at IFIC in Valencia in February 2009 for many interesting remarks. We are grateful to Jihad Mourad for discussions about the asymptotic bounded character of physical modes, and to Roberto Balbinot and Ted Jacobson for useful comments.

APPENDIX: ROLE OF DECAYING MODES

In this Appendix, our goals are, first, to show that in the black hole metric of Eq. (1), when using the dispersion relation Eq. (8) and for $\omega < \omega_{\max}$, the space of spatially bounded modes has dimension three, and second, to understand the physical roles of the decaying modes. In Sec. III C, when considering homogeneous flows, we saw that both growing and decaying modes should be discarded from the field operator. When the flow is only asymptotically constant, as is the case in Eq. (1), the symmetry between growing and decaying modes is broken because a mode that grows toward the horizon (we called this a "decaying" mode) does not necessarily grow in the other asymptotic region.

In the asymptotic supersonic region $x \to -\infty$ of Eq. (1), the wave equation reduces to the same form as in an homogeneous flow with velocity v_-. Thus, in this region, the general solution is a combination of all the exponential solutions that were present in the homogeneous case: four oscillatory solutions, $p-1$ decaying solutions, and $p-1$ growing solutions. This set defines the *mathematically* complete basis of modes $\{b^{\ell,a}_\omega(x)\}$ (thereafter called the "left" basis), where a labels the roots of Eq. (8) and ℓ stands for left, such that each $b^{\ell,a}_\omega$ has only one exponential component $e^{ik^a_\omega x}$ in the asymptotic supersonic region. When restricting ourselves to spatially bounded modes, the $b^{\ell,a}_\omega$ that correspond to growing components must be of course discarded. So one is left with $p+3$ independent modes bounded for $x \to -\infty$, numbered by $a = 1 \cdots p+3$.

In the subsonic asymptotic region, in general, these modes are not bounded because they are combinations of all exponential components, solutions of Eq. (8) with velocity v_+. On that side, one has p growing and p decaying modes, and only two oscillatory modes. In order to get modes that are everywhere bounded, one must consider combinations of the form

$$\tilde{\varphi}^{\,j}_\omega = \sum_{a=1}^{p+3} c^j_a b^{\ell,a}_\omega. \tag{A1}$$

The condition that the coefficients of the growing components in the subsonic region be all zero yields p constraints on the $p+3$ coefficients c^j_a. Therefore, only three linearly independent bounded combinations exist. In other words, the dimensionality of the space of spatially bounded solutions is three for $0 < \omega < \omega_{\max}$. This explains why only one extra mode was added in Eq. (19). It is also important to note that the p constraints in no way impose that the coefficients of the decaying modes be zero, and in fact the bounded modes, and, in particular, the ones constituting the in and out bases, generically contain decaying modes.

The physical role of these decaying modes is to "dress" the in and out modes in the region where $v(x)$ varies, in a way similar to the dressing of atoms by a local and nonpropagating polarization cloud when these are coupled to a radiation field [35]. Thus this dressing by decaying modes affects the properties of local observables (such as correlation functions) in the region where v varies.

For completeness, a word on the construction of the in and out bases is in order. Just as we constructed the left basis, we can construct a "right" basis $\{b^{r,a}_\omega\}$, from the asymptotic exponential solutions in the subsonic region. Looking at the space-time properties of wave packets made out of the asymptotically oscillatory modes in both $\{b^{r,a}_\omega\}$ and $\{b^{\ell,a}_\omega\}$, one can reclassify them into a group of three in modes and one of three out modes (still unbounded at this point). Each of these two groups mixes left and right modes. The dimensionality three of the space of bounded modes then ensures that we can find bounded combinations with only one in (respectively, out) mode with a nonzero coefficient. These combinations, suitably normalized and possibly complex conjugated to get a positive norm mode, yield the in (respectively, out) basis used in the text. Note also that since there are only two oscillatory solutions in the subsonic region, one (and only one, up to an overall factor) bounded mode exists that is purely decaying in this region. This mode, correctly normalized, is the CJ mode, here generalized to arbitrary (polynomial) dispersion.

[1] W. G. Unruh, Phys. Rev. Lett. **46**, 1351 (1981).
[2] T. Jacobson, Phys. Rev. D **44**, 1731 (1991).
[3] W. G. Unruh, Phys. Rev. D **51**, 2827 (1995).
[4] R. Brout, S. Massar, R. Parentani, and P. Spindel, Phys. Rev. D **52**, 4559 (1995).
[5] S. Corley, Phys. Rev. D **57**, 6280 (1998).
[6] Y. Himemoto and T. Tanaka, Phys. Rev. D **61**, 064004 (2000).
[7] H. Saida and M.-A. Sakagami, Phys. Rev. D **61**, 084023 (2000).
[8] W. G. Unruh and R. Schutzhold, Phys. Rev. D **71**, 024028 (2005).
[9] R. Balbinot, A. Fabbri, S. Fagnocchi, and R. Parentani, Riv. Nuovo Cimento Soc. Ital. Fis. **28**, 1 (2005).
[10] S. Corley and T. Jacobson, Phys. Rev. D **54**, 1568 (1996).
[11] W. G. Unruh, Proc. Sci. (QG-Ph)039 (2007).
[12] C. Barcelo, S. Liberati, and M. Visser, Living Rev. Relativity **8**, 12 (2005).
[13] T. Jacobson, S. Liberati, and D. Mattingly, Ann. Phys. (N.Y.) **321**, 150 (2006).
[14] R. Parentani, Phys. Rev. D **63**, 041503 (2001).
[15] R. Parentani, Int. J. Theor. Phys. **41**, 2175 (2002).
[16] P. Horava, Phys. Rev. D **79**, 084008 (2009).
[17] H. Yoshino and V. S. Rychkov, Phys. Rev. D **71**, 104028 (2005).
[18] J. Macher and R. Parentani, arXiv:0905.3634.
[19] T. A. Jacobson and G. E. Volovik, Pis'ma Zh. Eksp. Teor. Fiz. **68**, 833 (1998).
[20] R. Balbinot, A. Fabbri, S. Fagnocchi, A. Recati, and I. Carusotto, Phys. Rev. A **78**, 021603(R) (2008).
[21] I. Carusotto, S. Fagnocchi, A. Recati, R. Balbinot, and A. Fabbri, New J. Phys. **10**, 103001 (2008).
[22] S. Massar and R. Parentani, Phys. Rev. D **54**, 7444 (1996).
[23] R. Brout, S. Massar, R. Parentani, and P. Spindel, Phys. Rep. **260**, 329 (1995).
[24] T. G. Philbin *et al.*, Science **319**, 1367 (2008).

[25] R. Parentani, Classical Quantum Gravity **25**, 154015 (2008).
[26] J. Adamek, D. Campo, J. C. Niemeyer, and R. Parentani, Phys. Rev. D **78**, 103507 (2008).
[27] R. Schutzhold and W. G. Unruh, Phys. Rev. D **78**, 041504 (R) (2008).
[28] S. A. Fulling, *Aspects of Quantum Field Theory in Curved Space-Time* (Cambridge University Press, Cambridge, England, 1989).
[29] J. Macher and R. Parentani, Phys. Rev. D **78**, 043522 (2008).
[30] T. Jacobson and D. Mattingly, Phys. Rev. D **61**, 024017 (1999).
[31] W. G. Unruh, Phys. Rev. D **14**, 870 (1976).
[32] R. Parentani, Int. J. Mod. Phys. A **17**, 2721 (2002).
[33] U. Leonhardt, T. Kiss, and P. Ohberg, arXiv:gr-qc/0211069.
[34] C. Barcelo, L. J. Garay, and G. Jannes, Phys. Rev. D **79**, 024016 (2009).
[35] S. Massar, R. Parentani, and R. Brout, Classical Quantum Gravity **10**, 385 (1993).